

CHALMERS



Assessment of low-cost INS for positioning through sensor fusion with GPS

Master's Thesis within the Communication Engineering programme

OANA ROBESCU

Department of Radio Space and Science
CHALMERS UNIVERSITY OF TECHNOLOGY
Göteborg, Sweden 2010

MASTER'S THESIS

Assessment of low-cost INS for positioning through sensor fusion with GPS

Master's Thesis within the *the Communication Engineering* programme

OANA ROBESCU

SUPERVISORS:

Erik Steinmetz

Per Jarlemark

Ragne Emardson

EXAMINER

Jan Johansson

Department of Radio and Space Science
CHALMERS UNIVERSITY OF TECHNOLOGY

Göteborg, Sweden 2010

Assessment of low-cost INS for positioning through sensor fusion with GPS
Master's Thesis within the *the Communication Engineering* programme
OANA ROBESCU

© OANA ROBESCU, 2010

Department of Radio and Space Science
Chalmers University of Technology
SE-412 96 Göteborg
Sweden
Telephone: + 46 (0)31-772 1000

Cover:

The cover image shows the IMU that we used for the experiments. It is a product of Xsens and its code is MTi. More information are given in the report or can be found on the website www.xsens.com .

Chalmers Reproservice
Göteborg, Sweden 2010

Assessment of low-cost INS for positioning through sensor fusion with GPS
Master's Thesis in the *the Communication Engineering* programme
OANA ROBESCU
Department of Radio and Space Science
Chalmers University of Technology

ABSTRACT

Nowadays the most known and widespread application of GPS is the car navigation system. In order to use the GPS signal we need to be in open air, but what happens if we have to cross a tunnel, or an area where the signal cannot reach our receiver?

This master thesis project analyses the reliability of a system born from the sensor fusion of GPS with a low-cost Inertial Navigation System. This kind of system is able to keep track of the motion of the vehicle and estimate the position in real time, in order to keep the synchronization with the GPS signal, when this will be available again.

A regular GPS receiver and a low-cost INS are used; this last one contains three accelerometers and three gyroscopes.

The project can be divided in three main sections: an experimental part with the acquisition of data, a data pre-processing and noise estimation part in which data are synchronized and the noise effects are corrected, and a last part with the simulations, which are done using a Kalman filter to combine the two sets of data in a weighted form.

Key words: INS, IMU, GPS, sensor fusion, gyroscope, accelerometer.

Contents

ABSTRACT	I
CONTENTS	III
ACKNOWLEDGMENTS	V
LIST OF FIGURES	VI
LIST OF TABLES	VII
1 INTRODUCTION	1
1.1 Background	1
1.2 Aims of the project	1
1.3 Devices and software used	2
2 THEORY	3
2.1 GPS	3
2.1.1 Signals	3
2.1.2 Observables	4
2.1.3 DGPS	5
2.2 INS	6
2.2.1 Accelerometers	7
2.2.2 Gyroscopes	9
2.3 RFID	11
2.4 CAN	11
2.5 Sensor fusion	12
2.6 Kalman filter	14
3 EXPERIMENTS AND ACQUISITION OF DATA	17
3.1 The driving test	17
3.2 The acquisition system	18
3.2.1 MT Manager	20
3.2.2 PC View	21
4 DATA PRE-PROCESSING	23
4.1 Angular rates and Euler angles	23
4.2 Gravity compensation	23
4.2.1 Horizontal alignment	23
4.2.2 Removing of gravity components	26
4.3 Synchronization	27
4.3.1 Correlation	28
5 MEASUREMENT'S NOISE ESTIMATION	30

5.1	Standard deviation	30
5.1.1	Gyroscopes' data	30
5.1.2	Accelerometers' data	31
5.2	Allan deviation	32
5.2.1	Gyroscopes' data	33
5.2.2	Accelerometers' data	34
6	SIMULATIONS	36
6.1	Available Data	36
6.2	Generated Data	36
6.3	Modeling	38
6.4	Kalman filter: inputs and outputs	39
7	RESULTS AND COMMENTS	41
7.1	Horizontal position	41
7.2	Errors	46
8	DISCUSSION AND CONCLUSION	50
8.1	Discussion	50
8.2	Conclusion	50
9	REFERENCES	52

Acknowledgments

In this study, experiments with the INS and GPS have been carried out in April and May 2010 in SP Technical Research Institute of Sweden, Borås, Sweden.

This project has been carried out with Erik Steinmetz, Ragne Emardson and Per Jarlemark as supervisors, and Professor Jan Johansson as examiner. I would like to thank all of them for the help and support during these months, and for giving me the possibility to work in this team.

I also want to note that the experiments could never have been conducted without all the equipment and disposability of SP, and in particular the patience, and the car, of Erik Steinmetz.

Thanks to all the Earth and Space Sciences Department of Chalmers, and to my other colleagues, Carlos, Jana and Volker, for creating such a nice atmosphere in the office.

I would like to thank Gabriel Garcia, friend and colleague, for being always active in the experimental part of this thesis, and for making me smile despite some technical problems with the equipment or the software, and Mary, the best friend that I could have, for being so close to me despite the physical distance between us.

I also want to thank the “Erasmus team”: Berto, Sam, Pina, Andy, Filipe, Olga, Fufy, Francisco, Mehdi, Matt, Abhilash, Marta, Sumaiya, Alavi, Jorge, Pablo, Martin and all the others. They made my days sunny even with the rain or darkness, they embraced me when I was crying, and followed me when I was laughing, and without them everything would have been much harder.

A last thank you to my mother that made all this possible with her love and sacrifice, and to my family, far from me but always in my heart.

Göteborg, August 2010

Oana Robescu

List of Figures

- Figure 2.1 Strapdown inertial navigation algorithm
- Figure 2.2 A mechanical accelerometer
- Figure 2.3 A conventional mechanical gyroscope
- Figure 2.4 Loose coupling integration
- Figure 2.5 Tight coupling integration
- Figure 2.6 Deep coupling integration
- Figure 2.7 Sensor fusion architecture used in the project
- Figure 2.8 Kalman filter
- Figure 3.1 Map of the driving test
- Figure 3.2 Block diagram of the acquisition system
- Figure 3.3 Scheme for the synchronization of the data
- Figure 3.4 Picture of the system mounted on the car
- Figure 4.1 Horizontal misalignment between the body frame (b) and the global frame (G)
- Figure 4.2 Angles derived from gyro measurements and Euler angles after correction
- Figure 4.3 Removing of gravity components using the angles derived from the angular rates
- Figure 4.4 Removing of gravity components using the Euler angles
- Figure 4.5 Zoom of the North acceleration compensation results
- Figure 4.6 GPS and IMU yaw rate before the synchronization; resulting correlation function; GPS and IMU yaw rate after the synchronization.
- Figure 5.1 Sigma-tau diagram, Allan deviation
- Figure 5.2 Comparison between non-overlapping and overlapping methods
- Figure 5.3 Mod sigma-tau diagram, modified Allan deviation
- Figure 5.4 Allan deviation, X axis (Gyroscopes)
- Figure 5.5 Allan deviation, Y axis (Gyroscopes)
- Figure 5.6 Allan deviation, Z axis (Gyroscopes)
- Figure 5.7 Allan deviation, X axis (Accelerometers)
- Figure 5.8 Allan deviation, Y axis (Accelerometers)
- Figure 5.9 Allan deviation, Z axis (Accelerometers)
- Figure 7.1 Horizontal position, scenario 1.1
- Figure 7.2 Horizontal position, scenario 1.2
- Figure 7.3 Horizontal position, scenario 1.3
- Figure 7.4 Zoom of horizontal position, scenario 1.1
- Figure 7.5 Zoom of horizontal position, scenario 1.2
- Figure 7.6 Zoom of horizontal position, scenario 1.3
- Figure 7.7 Horizontal position, scenario 2.1
- Figure 7.8 Horizontal position, scenario 2.2
- Figure 7.9 Horizontal position, scenario 2.3
- Figure 7.10 East and north position errors, scenario 1.1
- Figure 7.11 East and north position errors, scenario 1.2
- Figure 7.12 East and north position errors, scenario 1.3
- Figure 7.13 East and north position errors, scenario 2.1
- Figure 7.14 East and north position errors, scenario 2.2
- Figure 7.15 East and north position errors, scenario 2.3

List of Tables

- Table 2.1 DGPS error sources
- Table 5.1 Standard deviation of gyroscopes' data
- Table 5.2 Standard deviation of accelerometers' data
- Table 6.1 Available Measurements
- Table 6.2 Generated data, used as input to the Kalman filter, and their origin
- Table 6.3 Scenarios used for the simulations
- Table 6.4 Kalman filter measurement modeling
- Table 6.5 Kalman filter state modeling
- Table 7.1 Maximum expanded measurement uncertainties for the different scenarios

1 Introduction

Nowadays the most known and widespread application of GPS is the car navigation system. In order to use the GPS signal we need to be in open air, but what happens if we have to cross a tunnel, or an area where the signal cannot reach our receiver?

This master thesis analyses the reliability of a system born from the sensor fusion of GPS with a low-cost Inertial Navigation System.

This kind of system is supposed to be able to keep track of the motion of the vehicle and estimate the position in real time, in order to keep the synchronization with the GPS signal, once this will be available again.

In this project other instruments have been used to complement to INS to aid the positioning algorithm during GPS outages: they are RFID position measurements and CAN speed measurements. The first ones represent points which position is known with high precision, comparable to the GPS one, where a vehicle, such as a forklift which drives in a covered industrial area, can check its own position. The second ones refer to a standard used on cars, and which evaluates the speed of the considered vehicle.

The experimental part of the project is carried out in SP Technical Research Institute of Sweden, in Borås.

1.1 Background

This project was born with the idea of integrating GPS measurements with other sensors measurements, in order to be able to track the position of a vehicle which is moving to an area where the GPS signal cannot be received: in fact in this case other positioning systems are needed and they all are combined with the available GPS data in order to obtain better future estimates of the vehicle position in the moment when the GPS signal disappears.

The project wants to find a solution for a very common problem: a vehicle that has to pass through a tunnel, or an industrial vehicle which drives in a partly covered area. In these cases the GPS is not enough to position the vehicle, so the sensor fusion is a reasonable option. But another important point is to consider the cost of such a device, and here a low-cost IMU is considered, to verify its stability and reliability, since it would be too costly to produce such integrations considering high performances IMUs, and of course they would not have big success on the market.

It is really interesting to study this kind of sensor fusion since it could be useful for many different applications, which include first of all in the automotive industry but also many other fields as seismic events detection or body motion analysis.

1.2 Aims of the project

The main aim of this project is to estimate the accuracy of an accurate positioning system using GPS data, and other data derived from these, and INS data. To achieve this it is necessary to achieve other minor goals: first of all it has to be solved the issue of the synchronization between the GPS receiver and the INS device in order to have

the possibility to set and do the experiments, and to obtain, from these, clear data ready to be processed and analysed.

After that it has to be done an estimation, and later a removal, of the noise on the data coming from the accelerometers and gyroscopes, as the bias or other thermo-mechanical noises.

In the end there are the simulations which involve the presence of a Kalman filter to combine the different sets of data in a weighted form, where it is possible to set the weighting factors and find the best solution.

To have good results three different sensors have been considered in the simulations: the IMU measurements have been integrated with RFID and speed measurements. In this way the precision of the positioning process during GPS outages can be increased.

The project, as the following report, can be divided in three main sections: the experimental part with the acquisition of data, the data pre-processing and noise estimation part in which data are synchronized and corrected, and the last part with the simulations where is possible to see the results of the project.

Later on different techniques and methods used are described in details.

1.3 Devices and software used

For this project two devices are used, which are a GPS receiver and an IMU (Inertial Measurement Unit).

The GPS receiver is produced by Javad and it can handle frequencies from 1 Hz up to 20 Hz. It has a 1 PPS port and an Event Input port, which can be used for synchronization. More information about it are given later on in the report or can be found on the web page www.javad.com.

The IMU is produced by Xsens, it is called MTi to identify the specific product and even being a low-cost model it has the basic features for this sensor fusion, which are the SyncIn and the SyncOut pins. It samples at 100 Hz, it contains three accelerometers, three gyroscopes and it can also map the magnetic field in order to better estimate where the magnetic north is to align the coordinate system. More detailed information about it are given later on in the report or can be found on the web page www.xsens.com.

Both the devices have a specific software that permits to control the sampling frequency and other settings, but they will be described in more detail in section 3.2.1 and section 3.2.2.

Another software that has been used to develop the project is Matlab, which helped to perform the simulations and the graphical results presented in the following chapters.

2 Theory

In this chapter some theoretical concepts are recalled to better understand the development of the project, described later on in this report.

First GPS is described, explaining the general principles of operation, and then a more detailed picture of all the segments and characteristics is given. In the end the error sources are listed and briefly described.

Then INS are introduced: accelerometers and gyroscopes are analyzed, explaining how they work, their possible characteristics and finally a description of the error sources is given.

Later a short description of RFID and CAN speed techniques is provided in order to have all the basis needed for the comprehension of the concept of sensor fusion, presented in the next paragraph.

In the end an introduction to the Kalman filter is provided with a general case filter description.

2.1 GPS

The Global Positioning System (GPS) is part of a satellite-based navigation system developed by the U.S. Department of Defence under its NAVSTAR satellite program (Grewal, Weill, & Andrews, 2007). This system has been declared fully operative in 1995. Nowadays the GPS is not just a military instrument anymore: in fact it is used for surveying, map-making, tectonics studies and of course for navigation.

The GPS can be divided in three segments: the space segment, the control segment, and the user segment.

The space segment consists of 30 satellites distributed over six orbits, each of those has an inclination of 55° over the Equator. In this way the orbital period of every satellite is of half sidereal day (≈ 11.967 h). The orbital planes are centred on the Earth in such way to have at least six satellites always visible from every point on the Earth's surface. Each satellite has four atomic clocks on board and broadcasts a one-way signal on two frequencies: $L1$ and $L2$ (Hofmann-Wellenhof, Lichtenegger, & Collins, 2001).

The control segment consists of a worldwide net of stations which control and monitor the health of the satellite constellation, uploads updated navigational data, maintains the satellites in their orbits sending occasional commands and adjusts the satellites' clocks.

The user segment consists of the GPS receivers which could be the military users of GPS Precise Positioning Service, or the civil Standard Positioning Service. The receivers include the antenna, the internal clock and a software able to calculate in real time the position of the user and the time associated to that position through the data coming from the received GPS signal.

2.1.1 Signals

Each GPS satellite carries a cesium and/or rubidium atomic clock to provide timing information for the signals transmitted by the satellites (Grewal, Weill, & Andrews,

2007). Every transmission is based on a fundamental frequency, which is $f_0 = 10.23$ MHz: in fact every satellite transmits an $L1$ signal with carrier frequency $f_1 = 1575.42$ MHz, and an $L2$ signal with carrier frequency $f_2 = 1227.6$ MHz.

There are three codes used: the C/A-code (Coarse Acquisition code) which is a relatively short, coarser-grained code having an associated clock, or chip, rate $f_0 = 1.023$ MHz, and it is 1023 chips long, before repeating, that means that its period is of 1 ms. Then there is the P-code (Precision code) which is a relatively long, fine-grained code having a clock, or chip, rate of $10f_0 = 10.23$ MHz, and period of 7 days (Grewal, Weill, & Andrews, 2007). In the end there is the Y-code which is obtained by multiplying the P-code by a W-code in order to obtain an encryption. It is also called anti-spoofing.

The C/A code is carried just by the $L1$ frequency, while the P-code is carried by both $L1$ and $L2$ frequencies. Both of them are Pseudo Random Number codes, but they are differently modulated: for C/A-code is used bi-phase modulation, while for P-code is used a quadrature modulation. In the combined signal P results 90° out of phase with C/A and it also has half of the power. The orthogonality of the codes gives the possibility to track satellites knowing only two codes out of three (Grewal, Weill, & Andrews, 2007)

The GPS satellite bit stream includes navigational information on the ephemeris of the transmitting GPS satellite, and an almanac for all GPS satellites, with parameters providing approximate corrections for ionospheric signal propagation delays (Grewal, Weill, & Andrews, 2007).

2.1.2 Observables

The GPS observables, also called ranges, are the distances between the satellites, with a known position in time and space, and the receiver. The range to each satellite can be determined by calculating the signal travel time, and multiplying it times the signal propagation speed, i.e. the speed of light.

The code generated in the satellite is synchronized with the atomic clock on board, which has a very high precision. When this code is received, the receiver generates a replica of it, synchronized with its clock, which is less precise than the atomic one.

Since the clock of the satellite is not synchronized with the clock of the receiver, and they have different precisions, the measure is biased by the clock errors. These biased ranges are called pseudoranges. Two simplified models of this can be seen in equation (2.1) and (2.2), referred respectively to the code difference and the phase difference.

$$R = \rho + c\Delta\delta t_r^s \quad (2.1)$$

$$\Phi = \frac{1}{\lambda}\rho + \frac{c}{\lambda}\Delta\delta t_r^s - N \quad (2.2)$$

Where R is the code pseudorange, ρ is the true distance and $c\Delta\delta t_r^s$ is the combined satellite receiver clock error (given in meters). In the phase model, Φ is the instantaneously measured phase in the receiver given in cycles, N , which is called the integer ambiguity parameter, is the remaining number of whole cycle between the

receiver and the satellite. The phase pseudorange is made up by $\phi + N$ and as mentioned N is an unknown parameter that has to be solved for before using the phase pseudorange. The code pseudorange is given in meters, while the phase pseudorange is given in cycles (Hofmann-Wellenhof, Lichtenegger, & Collins, 2001).

The position of the satellite is obtainable from the ephemeris, and the position of the receiver is obtainable from the data of four satellites: in fact it is known that in GPS a position has to be defined by three satellites for the three-dimensional position and by a fourth for the time measurement.

2.1.3 DGPS

Differential GPS (DGPS) is a technique for reducing the error in GPS-derived positions by using additional data from a reference GPS receiver at a known position. The most common form of DGPS involves determining the combined effects of navigation message ephemeris, ionospheric and satellite clock errors at a reference station and transmitting pseudorange corrections, in real time, to a user's receiver, which applies the corrections in the process of determining its position (Grewal, Weill, & Andrews, 2007).

This is the solution that would probably be used in a real case for this sensor fusion system. In the following section the error sources involved in these measurements are described.

2.1.3.1 DGPS error sources

The following error sources can be considered for both GPS and DGPS measurements, the difference is that in DGPS the error values determined by the base station are transmitted to the user and applied as corrections to the user's measurements. This is a limitation of DGPS, in fact the broadcast corrections are good only for users in a limited area surrounding the base station, outside this area the errors tend to be decorrelated, rendering the corrections less accurate (Grewal, Weill, & Andrews, 2007).

The most relevant factor for the inaccuracy of the GPS system is no longer an issue. On May 2, 2000 5:05 am (MEZ) the so-called Selective Availability (SA) was turned off. Selective availability is an artificial falsification of the time in the $L1$ signal transmitted by the satellite. For civil GPS receivers that leads to a less accurate position determination (fluctuation of about 50 m during a few minutes). Even if the reasons for using the selective availability were safety concerns, it is permanently deactivated due to the broad distribution and worldwide use of the GPS system (*The GPS System - Sources of Errors in GPS*, 2009).

Another factor influencing the accuracy of the position determination is the "satellite geometry", which describes the position of the satellites to each other from the view of the receiver. If the satellites giving a position are all concentrated in a relatively small area of the sky the Dilution Of Precision (DOP) is bad, while if they are distributed in the sky, the measurement is more reliable.

Although the satellites are positioned in very precise orbits, slight shifts of the orbits are possible due to gravitation forces. Sun and moon have a weak influence on the orbits. The orbit data are controlled and corrected regularly and are sent to the

receivers in the package of ephemeris data. Therefore the influence on the correctness of the position determination is rather low (*The GPS System - Sources of Errors in GPS*, 2009).

Another important factor is constituted by the multipath effect, which is caused by reflection of satellite signals (radio waves) on objects.

A very important error source is the atmosphere: in fact while radio signals travel with the velocity of light in the outer space, their propagation in the ionosphere and troposphere is slower. In the ionosphere electrons and positive charged ions are created by the ionizing force of the sun, and this layer refract the electromagnetic waves coming from the satellites, which will suffer of delays. These errors are mostly corrected by the receiver by calculations. The tropospheric effect is a further factor elongating the runtime of electromagnetic waves by refraction. The reasons for the refraction are different concentrations of water vapour in the troposphere, caused by different weather conditions. The error caused that way is smaller than the ionospheric error, but it cannot be eliminated by calculation.

As it has been said in the previous sections the receiver clock and the satellite clock cannot be really synchronized, so this causes an inaccuracy in time which corresponds to an error in the position determination.

Finally it has to be added the random noise, which cannot be quantified since it affects the errors listed before in a random way.

In the following table the position errors produced by the listed sources on the GPS measurements are summarized and approximately quantified.

Table 2.1 DGPS error sources

Source	Error magnitude
Satellite orbits	± 2.5 [m]
Multipath effect	± 1 [m]
Ionospheric effects	± 5 [m]
Tropospheric effect	± 0.5 [m]
Satellite clocks	± 2 [m]

2.2 INS

INS (Inertial Navigation Systems) are based on a self-contained navigation technique in which measurements provided by accelerometers and gyroscopes are used to track the position and orientation of an object relative to a known starting point, orientation and velocity (Woodman, 2007).

For this project it is used an IMU (Inertial Measurement Unit) which contains three orthogonal accelerometers and three orthogonal gyroscopes, to measure linear acceleration and angular velocity with high data rate and bandwidth.

INS can be divided in two categories which differ in the frame used, and consequently in the navigation algorithm used. To better understand this concept it is needed to briefly define the *body frame* as the frame of the navigation system, and the *global frame* as the frame in which the navigation takes place. The first category includes Stable Platform Systems: the inertial sensors are mounted on a platform which is isolated from any external rotational motion (Woodman, 2007). In this case it is possible to obtain the orientation of the device directly from the gyroscopes, and the velocity from the accelerometers, double integrating the output data (after a correction for gravity on the vertical axis). The second category, which is the case of this project, includes Strapdown Systems: the inertial sensors are mounted rigidly onto the device, and therefore output quantities measured in the body frame rather than the global frame (Woodman, 2007). So in this situation the orientation is still obtained directly from the gyroscopes, but to calculate the velocity it is needed first to project the accelerations on the global axes, as shown in Figure 2.1, then it is possible to proceed with gravity correction and double integration.

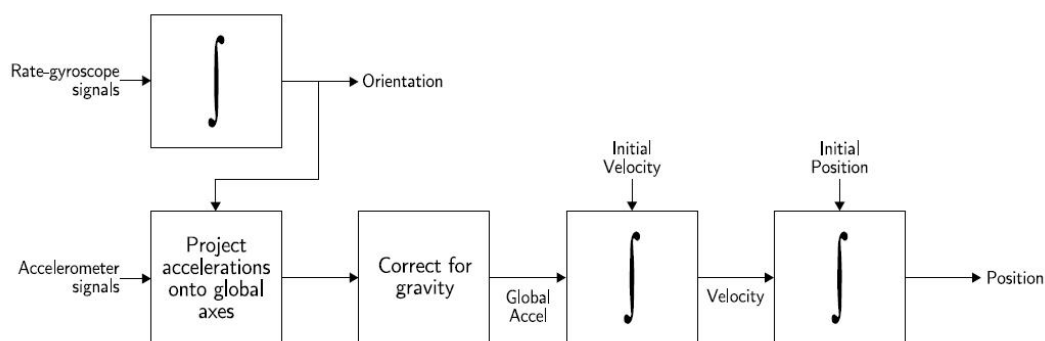


Figure 2.1 Strapdown inertial navigation algorithm

2.2.1 Accelerometers

Nowadays accelerometers are very diffused because of the large number of possible applications, but also because of the small size recently reached by the manufacturing market. They can be used to measure vehicle acceleration, as in this project, to measure vibrations on cars, buildings, process control systems, to measure seismic activity, inclination or for machinery health monitoring of rotating equipment such as pumps, fans or compressors (Wikipedia - Accelerometer, 2010).

Accelerometers can be classified as mechanical or solid state devices. This project involves the use of solid state accelerometers.

Most micromechanical accelerometers operate in-plane, which means that they are designed to be sensitive only to a direction in the plane of the die (Wikipedia - Accelerometer, 2010). Conceptually an accelerometer consists of a proof mass suspended by springs, as shown in Figure 2.2.

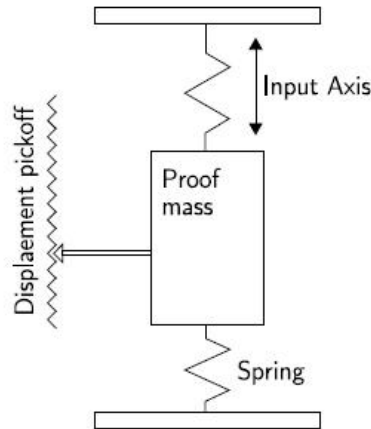


Figure 2.2 A mechanical accelerometer

When the proof mass experiences an acceleration along the input axis, it will be displaced from its equilibrium position. This displacement is measured using a displacement pick-off, giving a signal that is proportional to the force F acting on the mass in the direction of the input axis. Newton's second law (2.3) is then used to calculate the acceleration acting on the device (Woodman, 2007).

$$F = m \cdot a \quad (2.3)$$

The equilibrium position of the proof mass is calibrated for zero acceleration; an acceleration in the plus direction causes the mass to move downwards with respect to the case, and this indicates a positive acceleration. Now imagine that the accelerometer is sitting on a bench in a gravitational field, in this case the proof mass is again displaced downward with respect to the case, but the gravitational acceleration is downward. Therefore, the output of an accelerometer due to a gravitational field is the negative of the field acceleration (Stovall, 1997). In order to better estimate a possible initial tilt of the accelerometer, the static acceleration exerted by the gravity can be studied. This is part of a method called "Horizontal alignment" which is used in the project and detailed described in Section 4.1.1.

In commercial devices it is possible to have piezoelectric, piezoresistive or capacitive components to convert the mechanical motion into an electrical (analog or digital) signal. Piezoresistive accelerometers are preferred in high shock applications, while capacitive accelerometers reach better performances in the low frequency range (Wikipedia - Accelerometer, 2010).

2.2.1.1 Error characteristics

Measurements produced by mechanical accelerometers contain errors due to the mechanical nature of the sensor: it follows a short description of the error characteristics of an accelerometer.

First of all it has to be considered the *constant bias*, which consists of the offset of the output value from the true value, and it can be considered constant over a short period

of time. A constant bias error of ϵ , when double integrated, causes an error in position which grows quadratically with time (Woodman, 2007). This bias can be estimated when the device is standing, so it is not subject of any acceleration, but it has to be known the exact position of the device with respect to the gravitational field because there are components of the gravity which can appear as a bias.

The bias influences also the temperature of the device with its fluctuations, but the temperature itself depends on the single device since changes in temperature are due to the friction between two, or more, parts. In the IMU used in this project there is a temperature sensor which can be used to compensate for these errors, but it has to be used carefully because it is not possible to separate the two effects, and understand which temperature rise is due to the bias.

The output values of an accelerometer contain also a *thermo-mechanical white noise* sequence, which produces, after a double integration, a *random walk* in position, with zero mean and a standard deviation which grows proportionally to $t^{3/2}$.

Mechanical accelerometers are also subject to *flicker noise* which creates a second order random walk in velocity whose uncertainty grows proportionally to $t^{3/2}$, and a third order random walk in position which grows proportionally to $t^{5/2}$ (Woodman, 2007).

In the end there are *calibration errors* such as *scale factor errors*, linear errors proportional to the input signal, or *misalignments*, which refer to the mechanical alignment error of each sensor to the platform axes and are described as a random constant (Stovall, 1997). They can be observed only when the device is subject of an acceleration, and they look like bias errors.

All these errors are idealizations: for example, bias errors are only constant for short terms, they typically exhibit drift that might be modeled as a Markov process superimposed on a constant bias (Stovall, 1997), but to be able to remove them, at least partially, the models just listed are usually used.

2.2.2 Gyroscopes

The first gyroscope was built by Foucault in 1852 and used for an experiment involving the rotation of the earth. Then the spinning mass gyroscope first found a home around 1920 in the single-degree-of-freedom rate gyro used as a basic turn indicator for instrument flying (Barbour, Elwell, & Setterlund, 1992). After that the main application of gyroscopes was always considered to be for aircraft and flight control systems, since they provide information about the orientation of the device they are mounted on.

As for the accelerometers, it is possible to have two different types of devices: mechanical or optical gyroscopes.

A conventional mechanical gyroscope is based on the principle of conservation of angular momentum, and it basically consists of a spinning wheel mounted on two gimbals (Figure 2.3) which allow it to rotate in all three axes (Woodman, 2007).

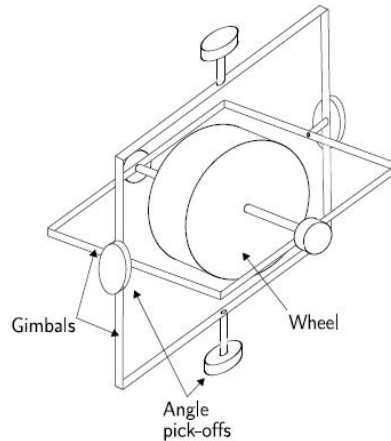


Figure 2.3 A conventional mechanical gyroscope

The spinning wheel resists to changes in orientation, hence when the gyroscope is subject to a rotation the wheel remains at a constant global orientation; just the angles between adjacent gimbals change, and this difference is measured with angle pick-offs. In this way the information that is given as output is about orientation. But it is much more common to find on the market devices, called rate-gyros, which give orientation information in form of angular velocity.

The fiber optic gyroscopes (FOG) measure angular velocity using the interference of light: two light beams are fired into the coil in opposite directions; if the sensor is undergoing a rotation then the beam travelling in the direction of the rotation will experience a longer path to the other end of the path than the beam travelling against the rotation, and this is known as Sagnac effect (Woodman, 2007).

2.2.2.1 Error characteristics

Measurements produced by mechanical gyroscopes contain the same errors analyzed in the case of the accelerometer, but it is needed anyway a brief description since now the outputs are angular velocities and not velocities.

First of all it can be observed a *constant bias*, that is the offset of the output from the true value, when the device is not subject of any rotation, and this is expressed in $^{\circ} / h$. When it is integrated it causes an angular error which grows linearly with time (Woodman, 2007). As for the accelerometers, it can be estimated when the device is standing, and then it just has to be subtracted from the output. It has to be considered again the temperature effect on the bias: due to the friction between mechanical parts, and due to changes in the environment where the device is acting, the temperature can change inducing fluctuations in the bias.

Also for gyroscopes there is a *thermo-mechanical white noise* which disturbs the output values, and which fluctuates at a rate much greater than the sampling rate of the sensor (Woodman, 2007). This noise, after the integration, introduces a zero-mean random walk error with a standard deviation which grows proportionally to the square root of time.

Mechanical gyroscopes are also subject to *flicker noise*, which has a $1/f$ spectrum, and which effect, observable at low frequencies, is the fluctuation of the bias,

described by the *bias stability*. This last one describes how the bias of a device changes in time under unchanged conditions, and integrating the fluctuations it is obtained a second-order random walk in angle. Indeed the bias fluctuations are not totally random, since they have to be in a certain range, otherwise the drift would grow too much in a very short period of time.

In the end there are also for gyroscopes the *calibration errors* analyzed in section 2.2.1.1, which appear in the form of bias errors observable just when the device is undergoing a rotation.

The same considerations made for accelerometers' error characteristics can be applied in this case, since also these errors can be described by stochastic processes.

Considering all these errors it is easy to understand why INS can be a support for GPS navigation systems, but cannot replace them since their reliability decays very fast in time. This will be confirmed later on when the results of the experiments will be presented in chapter 7.

2.3 RFID

Radio-frequency identification (RFID) is a technology that, through wireless radio-frequency sensors, permits to identify and locate object, animals or people.

Radio -frequency identification involves interrogators, also known as readers, and tags, also known as labels. The tags can be read from several meters away and they contain at least two parts, which consist of an antenna which receives and transmits the signal, and an integrated circuit which stores and processes the information.

In this project it has been thought to an industrial vehicle, for example a forklift, driving on a path, which includes some RFID points: the forklift can have an interrogator on board, so when it passes close enough to these points it can read their tag and know its own exact position.

It will be later described how these measurements have been obtained in this specific case.

2.4 CAN

Controller area network (CAN) is a serial bus system standard introduced 1983 by Robert Bosch GmbH. It was devised to control actuators and receive feedback from sensors.

The CAN bus can be used to connect engine control unit and transmission, or different controls (climate control, seat control, etc.). But nowadays it is also used as a fieldbus in general automation environment.

In this project it is supposed to be used to transport the information about the speed of the vehicle, which is detected by some sensors, and the resulting measurements are supposed to have a high precision.

It will be later described how these measurements have been obtained in this specific case.

2.5 Sensor fusion

The expression *sensor fusion* is referred to the integration of two or more sensors' outputs: in this case it refers to the integration of the outputs of GPS, INS, RFID and CAN speed sensors, which are combined in order to better estimate the true value, moment by moment.

The primary output of a GPS receiver is the position of its antenna relative to an earth-centered coordinate system, and the position errors can depend on the availability and geometric distribution of the satellites that can be tracked, and other error sources described in section 2.1.3. The primary output of an INS is the position of the sensor in the INS coordinate system, and the position errors can depend on the quality of the inertial sensors, the earth model used and other error sources described in sections 2.2.1.1 and 2.2.2.1 (Grewal, Weill, & Andrews, 2007).

The errors of a GPS are usually bounded, those of INS use to grow in time without any bound, so due to this complementary error behaviour of both sensors, it is possible to reach higher performance levels, but the gain in accuracy, availability, integrity and continuity depends also on the architecture of integration (Kreye, Eissfeller, & Ameres).

Usually there are three different architectures of integration which depend on the type of information shared between the two sensors: “*loose-*“, “*tight-*“ and “*deep-coupling*”. Hereafter these techniques are described.

In the case of a loose coupled integration the two sensors produce two independent solutions for the position, which are combined by a Kalman filter providing on one hand estimations of integrated navigation solution, and on the other hand current error states of the inertial sensor like biases or scale factors; these errors are used in a recursive way to improve the accuracy of the inertial navigation solution (Kreye, Eissfeller, & Ameres) as it is shown in Figure 2.4.

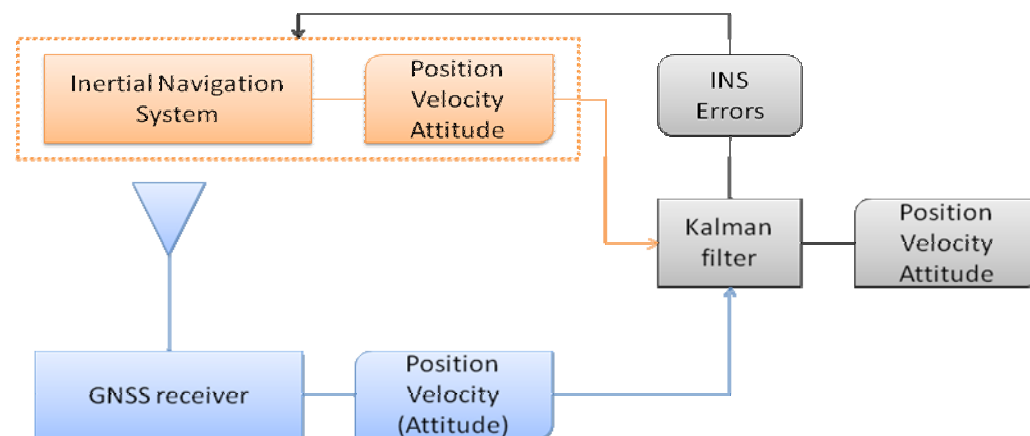


Figure 2.4 Loose coupling integration

In this way it is possible to increase the accuracy of the system since INS acts as a filter on the noise effects, and during GNSS outages the position is given by INS.

A second possibility is to have a tight coupling integration. In this case the GNSS receiver has an additional input which is a feed-back coming from INS solutions; these data go directly into the tracking loop of the receiver so then both pseudoranges are processed in a filter, which makes the global system to have better performances depending on the quality of the INS. The Figure 2.5 shows a scheme of this integration architecture.

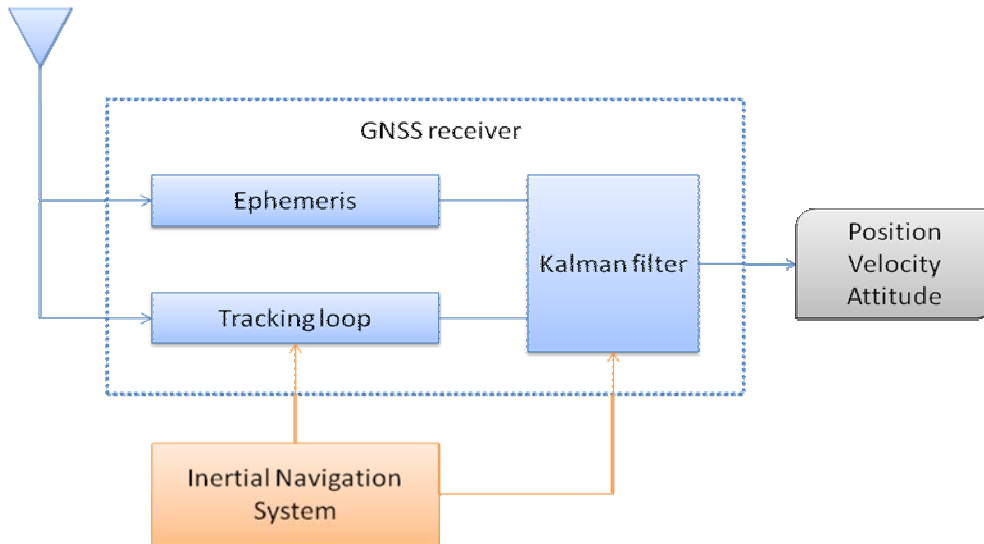


Figure 2.5 Tight coupling integration

Because of the complex relationship between the measurements and the error states, this integration has a weaker degree of observability (Salytcheva, 2004).

In the end it is possible to have a deep coupling (also called “ultra-tight” coupling) integrated system, in which case GNSS and INS work as a unique system and the integration filter is included in the tracking loop of the receiver, which now depends on the INS itself. This system is shown in Figure 2.6.

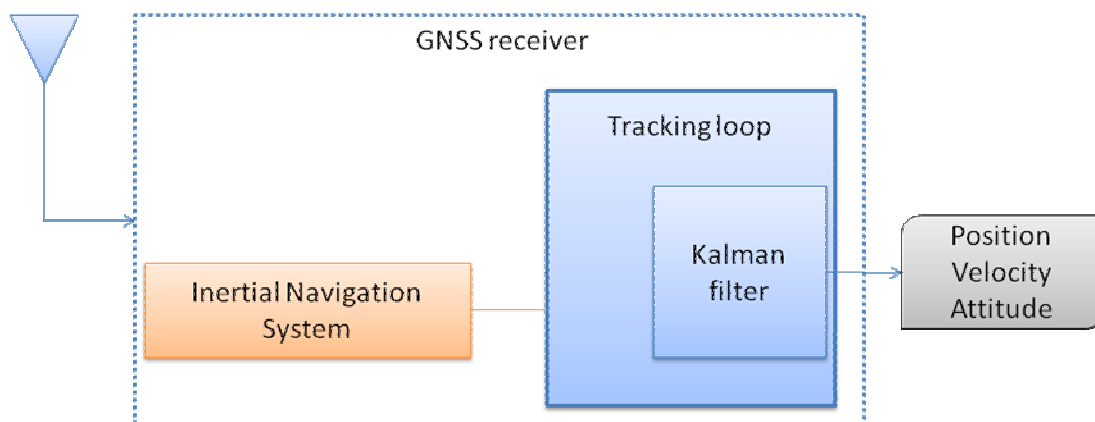


Figure 2.6 Deep coupling integration

Using this architecture can be noticed a gain in robustness to GNSS outages either due to vehicle dynamics, interference, or jamming. However the major drawback of this scheme is the complexity involved in integrating INS information deep inside the receiver (Wieser & Gebre-Egziabher, 2007).

In this project no one of the architectures described was used, even though it was very similar to the loose coupling technique, and it shown in Figure 2.7.

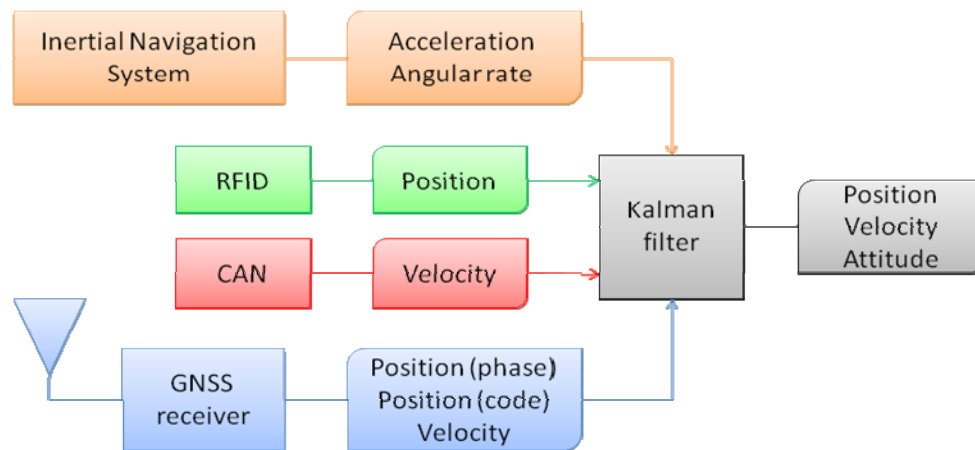


Figure 2.7 Sensor fusion architecture used in the project

This architecture and the scheme in Figure 2.7 will be described in detail in section 6.

2.6 Kalman filter

In 1960 R.E. Kalman published a paper describing a recursive solution to the discrete-data linear filtering problem. Since that time, due in large part to advances in digital computing, the Kalman filter has been the subject of extensive research and application, particularly in the area of autonomous or assisted navigation (Welch & Bishop, 2006).

The Kalman filter is a recursive filter and it estimates the state of a process, in a way that minimizes the mean of the squared error: in fact it specifies how the inputs should be weighted in order to have the best estimation of the current, or required, output. This filter is very powerful in several aspects: it supports estimations of past, present, and even future states, and it can do so even when the precise nature of the modeled system is unknown (Welch & Bishop, 2006). It is similar to the Wiener filter and based on the same principles, but the Kalman filter can handle better discrete data problems.

A general problem solved with Kalman filter is to estimate the state $x \in \mathfrak{R}^n$ of a discrete-time controlled process, governed by the following equation:

$$x_k = Ax_{k-1} + Bu_{k-1} + w_{k-1} \quad (2.4)$$

with a measurement $z \in \mathfrak{R}^m$ such as

$$z_k = Hx_k + v_k \quad (2.5)$$

The random variables w_k and v_k represent the process and measurement's noise: independent of each other, white and with normal probability distributions:

$$p(w) \sim N(0, Q) \quad (2.6)$$

$$p(v) = N(0, R) \quad (2.7)$$

Where Q is the process noise covariance, and R the measurement noise covariance: these two matrices should change with each time step, but now they are assumed to be constant. The same is valid for the matrices A , B and H .

To continue it has to be defined $\hat{x}_k^- \in \mathbb{R}^n$ as the *a priori* state estimate at step k , given knowledge of the process prior to step k , and $\hat{x}_k \in \mathbb{R}^n$ as the *a posteriori* state estimate at step k , given the measurement z_k .

The *a priori* and *a posteriori* errors are defined as follows:

$$e_k^- = x_k - \hat{x}_k^- \quad (2.8)$$

$$e_k = x_k - \hat{x}_k \quad (2.9)$$

and the *a priori* and *a posteriori* estimate error covariance are then:

$$P_k^- = E[e_k^- e_k^{-T}] \quad (2.10)$$

$$P_k = E[e_k e_k^T] \quad (2.11)$$

The goal now is to find an expression of the *a posteriori* state estimate as a linear combination of the *a priori* state estimate, shown in the following equation:

$$\hat{x}_k = \hat{x}_k^- + K(z_k - H\hat{x}_k^-) \quad (2.12)$$

where the difference $(z_k - H\hat{x}_k^-)$ is called the *measurement innovation* or the *residual*. It reflects the discrepancy between the predicted measurement $H\hat{x}_k^-$ and the actual measurement z_k .

K is chosen to be the *gain* or *blending factor* that minimizes the *a posteriori* error covariance (2.11). One possible resulting K is given by:

$$K_k = P_k^- H^T (H P_k^- H^T + R)^{-1} \quad (2.13)$$

As the measurement error covariance R approaches zero, the actual measurement z_k is trusted more and more, while the predicted measurement Hx_k^- is trusted less and less. On the other hand, as the a priori estimate error covariance P_k^- approaches zero the actual measurement z_k is trusted less and less, while the predicted measurement Hx_k^- is trusted more and more.

The Kalman filter estimates a process by using a form of feedback control: the filter estimates the process state at some time and then obtains feedback in the form of (noisy) measurements (Welch & Bishop, 2006). So the equations related to it are divided in two groups: time update equations and measurement update equations. The first group concern the projection in the future of the current state and its relative error covariance estimates to obtain the *a priori* estimates in the next step, while the second group concern the feedback: they incorporate a new measurement into the *a priori* estimate to obtain an improved *a posteriori* estimate (Welch & Bishop, 2006).

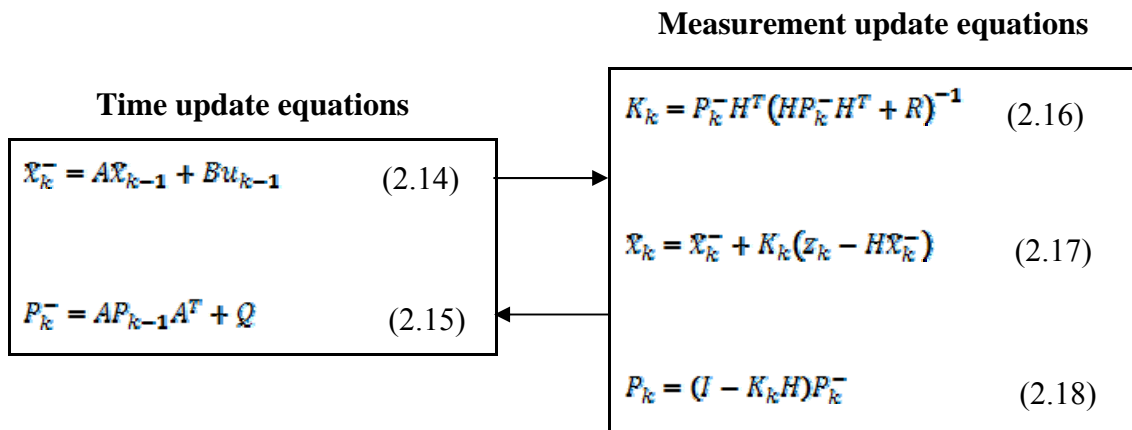


Figure 2.8 Kalman filter

In the project it has been used an extended Kalman filter which follows the same principles of a regular Kalman filter but which can deal with non-linear models.

3 Experiments and acquisition of data

In this chapter the experiments and the acquisition of data are presented: first a description of the driving test is given, including a map of the route and the criteria used to choose the route itself. Later the acquisition system is described: what the physical system was composed by, how it was mounted on the car and how it worked. In the end a description of the software used for the acquisition of INS and GPS data is provided, to better understand which are the possibilities and the limits of this system built with these specific devices.

3.1 The driving test

The initial idea for this project has been to use a robot, to be precise a mechanical arm, which can be programmed to execute a certain sequence of movements with a certain speed, and to mount on its end the GPS receiver and the IMU. Unfortunately, due to technical problems, this has not been possible so the second alternative was to mount the whole system on a car and drive on a determined path.

The driving test was carried out on the 10th of May in an industrial area in Borås, close to the SP's venue, and the designed path is shown in Figure 3.1. In order to have the possibility to do compensations and noise characterizations, described in sections 4 and 5, the test includes one initial minute in which the car is not moving.

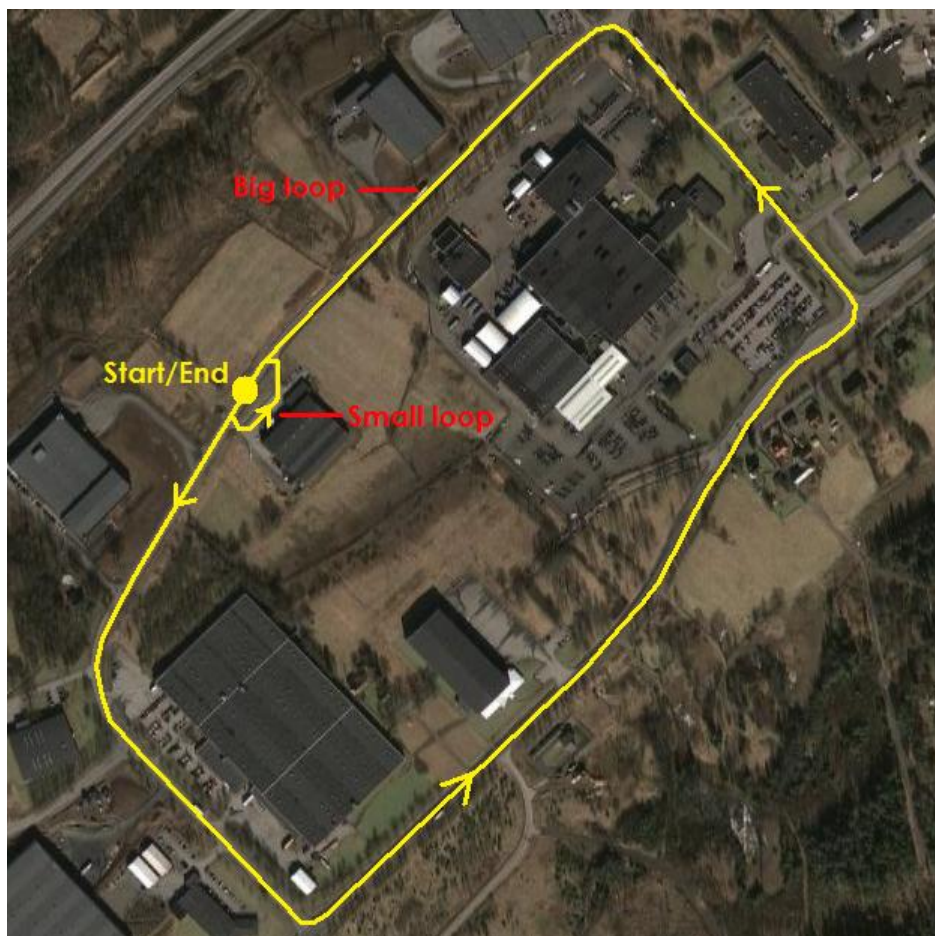


Figure 3.1 Map of the driving test

3.2 The acquisition system

The acquisition system used in this project consists of the following elements:

- one GPS receiver
- one IMU
- one battery backup
- one laptop

It follows a short description of each element of the previous list.

The GPS receiver used is produced by Javad. It is a GPS and GLONASS receiver, its maximum sample rate is of 20 Hz, 1 PPS can be set rise or fall edge and it has two external event markers which react to events registered on the port “FRQ In/Out”. All the files containing the measurements are stored directly in the internal memory of the receiver itself, and an USB port allows to connect the receiver to the laptop to process the data.

The IMU used is the MTi produced by Xsens. It is a complete miniature inertial measurement unit with integrated 3D magnetometers (Xsens, 2007), its maximum sample rate is 512 Hz for raw data, and 120 Hz for processed data; in this case the sample rate used is 100 Hz. The synchronization functions deserve to be described in detail: this IMU has two pins called SyncIn and SyncOut respectively, which give the possibility to synchronize the IMU itself with an external clock source, in the first case, or to synchronize another device on its internal clock, in the second case. These two functions can be enabled in the same time so the IMU can wait for an input pulse and then send an output pulse when it starts sampling, and this is exactly the purpose of this part of the project. The two synchronization functions can have different properties such as positive or negative pulse, or the pulse width in the case of the output, but the most important is the skip factor: this indicates how many times the trigger has to be skipped before actually trigger the device.

The battery backup is given by the laboratories of SP and it provides 12 or 24 V which have been used to power the GPS receiver.

The laptop has been used to capture the data with the software which will be presented in the following sections, 3.2.1 and 3.2.2, and to process and analyze the results of the experiment.

The first problem which has to be solved was the synchronization of the two sensors: in fact the objective was to collect data from the GPS receiver and from the IMU in the same time, to have the possibility to introduce them in the Kalman filter to combine them. Of course it is not possible to start the two measurements in the same time just manually, because the delay between them would be too large.

For this purpose it has been decided to use the synchronization functions: the 1 PPS and one external event marker for the GPS receiver, and the SyncIn and SyncOut pins for the IMU. To make this system work it has been chosen to consider the GPS receiver as the master and the IMU as the slave, since the internal clock of the receiver has much higher precision than the one of the IMU.

The first step consists of connecting the two devices to each other and to the laptop, and setting the parameters in a way that the communication between themselves is possible: so the “1 PPS” port of the receiver is connected to the “SyncIn” pin of the

IMU, the “FRQ In/Out” port of the receiver is connected to the “SyncOut” pin of the IMU to register external events coming in the GPS receiver, and the two USB ports are connected to the computer as shown in Figure 3.2.

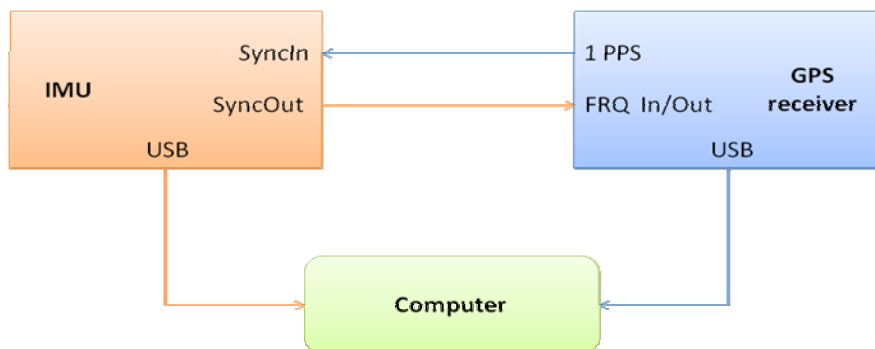


Figure 3.2 Block diagram of the acquisition system

After this the IMU has to be set in the following way: the SyncIn has to be enabled on the rising edge, with no skip factor, the SyncOut has to be enabled as a positive pulse of width of 5 ms, with no skip factor. Then the IMU has to be set in “Configuration mode” which means that, if any input signal comes, it does not recognize it since it has to be configured still.

Now for the GPS receiver it has to be configured, but not enabled, the PPS A with a period of 10 ms, to have the same frequency of the IMU, on the rise edge and with reference time of GPS.

Finally it is possible to start the acquisition of the data: first of all the GPS receiver starts to record data, when the PPS A is not enabled yet, after that the IMU has to be set in “Measurement mode”, which means that even if the recording is on, it will wait for an incoming signal to actually start to record data. In the end the PPS A from the receiver is enabled, so it sends a 100 PPS to the IMU, and this one starts to record and sends, in the same time, the SyncOut pulse. In this way it is possible to synchronize the two devices, since in the file obtained from the receiver the SyncOut will appear as a “Marked external event” and it will specify the exact time of it, so it will be possible to remove the data recorded by the GPS receiver before the synchronization started and after the IMU stopped recording (Figure 3.3).

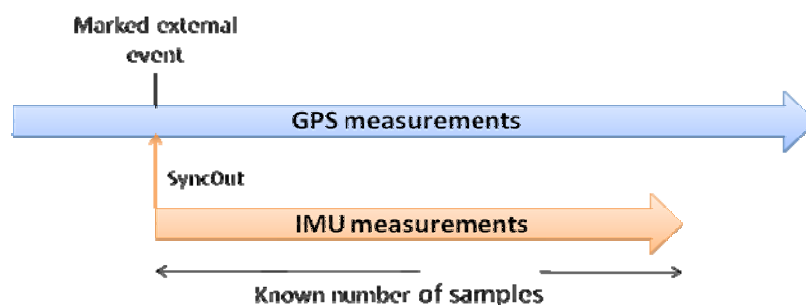


Figure 3.3 Scheme for the synchronization of the data

The acquisition system, described in Figure 3.2 was mounted on a car for the driving test: the receiving antenna and the IMU have been fixed on a wooden base and this one has been positioned on the car roof and held by two belts. Since the car could introduce vibrations and, in this way, compromise the measurements, some pieces of foam and other similar materials were introduced between the car roof and the wooden base, as show in the picture in Figure 3.4.



Figure 3.4 Picture of the system mounted on the car

The rest of the system has been mounted inside the car, and the cables from the IMU and from the antenna passed through the window, as it can be seen from Figure 3.4.

3.2.1 MT Manager

MT Manager is a software produced by Xsens and it permits to control the IMU before, during and after the experiments. It gives the possibility to configure the IMU as soon as it is connected to the computer, without need to do it afterwards using the specific menus.

This platform permits to choose the scenario in which the IMU has to work, which can be “Human”, for slow movements, “Human large acceleration”, for impacts, “Machine”, for situations in which the accelerations are slower and of longer periods of time than for the Human case, “Machine no magnetic field”, for situations in which the magnetic field is too distorted to be useful for the stabilization, and “Marine”, for slow, long term accelerations and mild magnetic disturbances. Another characteristic which can be set is the oriented output mode: it is possible to choose between “Quaternions”, which is a four dimensional vector space, “Euler angles”, which gives as output the rotation of the three axes called roll, pitch and yaw, and “Rotation matrix”, also known as direction cosine matrix. In addition to this it can be selected to have “Raw” or “Calibrated” data; this last mode implies that the raw data have been corrected and calibrated following a physical model of the response of the sensors to various physical quantities (Xsens, 2007). It is also possible to control other parameters such as the SyncIn and SyncOut functions, or to set the format of the

output files even if a specific oriented output mode is used, for example using the Euler angles it is still possible to recover the data in the other formats and have them printed in a .txt file.

For this experiment it has been chosen to use the “Machine no magnetic field” scenario, since the system was on a car, and the test carried out in a industrial area, which conditions could distort too much the magnetic field. The accelerometers’ data were used, and both the gyroscope calibrated measurements and the Euler angles to estimate the rotations: this because the data coming from the gyroscope are calibrated but they consist of angular velocities in rad/s, so to estimate the angles an integration is needed, and this could introduce some errors, while using the Euler angles this problem is avoided, since the data already consist of angles, but still they could be a little less precise not containing any calibration. In section 4 they will be better compared to understand which one could be the best choice.

Once all the settings are done it is possible to control the behaviour of the IMU using the low level communication tool: in this way it is possible to set it in Configuration or Measurement mode, to start the recording or to stop it. Furthermore it possible to see the developing of the motion in real time in many different ways: there is a 3D representation of the IMU, which reproduces on the screen the motion sensed in a Cartesian axes system, a roll-pitch-yaw representation, which shows three subplots with the behaviour of the three axes, or an acceleration representation, which shows the developing of the three accelerations in three different colours.

One last useful tool of this software has been the option to play a recorded file: in fact it has been used to check in a fast way the car vibrations without need of processing the data with the use of Matlab. In this way it has been possible to check the best positioning of the system before doing the very last experiment.

The file produced and managed with this software is a .txt file and the settings have been chosen in order to have calibrated data. The files used in the next part of the project contain a heading to specify the start time, the sample rate, the scenario and the firmware version; after this they are divided in nine columns: in the first three columns there are the instantaneous accelerations for the three axes, in the next three columns there are the angular velocities for the three axes and in the last three the magnetic field measurements for the three axes.

Regarding the Euler angles, the software produces another file which starts with the same heading as the previous one, but after this it has just three columns with the instantaneous angle values, with respect to the Cartesian East-North-Vertical (ENV) coordinate system, for the three axes: they are referred to as roll, pitch and yaw, and they are expressed in degrees.

3.2.2 PC View

This software is produced by Javad, as the receiver and it gives the possibility to connect the receiver to a computer and control several settings of the receiver itself.

First of all it is possible to track all the visible satellites, GPS and GLONASS, and to know their status in real time. There is also the current position of the receiver displayed in real time and it includes also the time-frequency parameters which describe the behaviour of the receiver’s local oscillator. The current position can be given either in geodetic coordinates, or in Cartesian coordinates.

Moreover other settings can be controlled with PC View such as the sampling rate of the receiver, the frequency source, which can be internal or external, and the PPS events, which can have a frequency or can be set to appear just once.

Through the software it is also possible to start and stop the recording of measurements and download the files on the computer, using the “File manager menu”. The files are automatically saved in .jps format, which has to be later converted into RINEX (Receiver Independent Exchange) format. This kind of format first of all contains a header which gives global information for the entire file such as the starting time of the measurement, the initial position, the antenna type, the number and name of the visible satellites, and a list of the parameters contained in the file for every satellite. In this case for every satellite, for every sample, were available the following parameters: the observation time, which is the receiver time of the received signal, the pseudorange, called C1, the C/A code derived carrier phases called L1 and L2, the P code derived carrier phases called P1 and P2, and the Doppler called D1 and D2.

4 Data pre-processing

As it has been described in section 3.2, the system is composed by two main parts, the GPS receiver and the IMU, which both produce a file containing the calculated position of the car. These two files will later be merged, but the IMU file still needs some corrections: in fact the measurements still contain gravity components and biases. The gravity compensation and a post-experiment synchronization are described in this chapter.

4.1 Angular rates and Euler angles

Before describing the methods used for correcting the IMU measurements, it is useful to explain which kind of data can be obtained by this device.

As mentioned in section 3.2.1, it is possible to obtain, as output, different data: in detail it is possible to have angular rates or Euler angles.

The first come from the “Calibrated” output mode, and they consist of raw gyroscope data calibrated according to a physical model of the response of the sensors to various physical quantities, such as temperature (Xsens, 2007).

The second one comes from the Xsens Kalman Filter (XKF): gravity and magnetic field measurements compensate for the drift errors produced by the angular rate’s integration. In this specific case the magnetic field is not acting since it has been used the “Machine no magnetic field” scenario as described in section 3.2.1.

In the next section it will be possible to observe the differences between these two formats of angular information, and compare the results with the two methods.

4.2 Gravity compensation

When the system has been mounted on the car, a spirit-level has been used to position it horizontally, but of course it is not possible to do it perfectly if it is manually done. Therefore in the data can be found gravity components or biases due to calibration errors. In the following sections the techniques used to remove these errors are described.

4.2.1 Horizontal alignment

Horizontal alignment is the procedure for computing the initial misalignment angles in horizon $\theta_x(\mathbf{0})$ and $\theta_y(\mathbf{0})$ (Salytcheva, 2004) which will be later used to remove gravity components from the accelerations. In the ideal situation, when the IMU’s axes directions are perfectly aligned with the global frame, the accelerometers should measure the gravity on the vertical axis, and zero on the other two axes, while the gyroscopes should measure zero on all the axes, for an inertial frame. In real situations this does not happen so it is necessary to compensate for misalignments and biases occurring because of many reasons, as it has been said in section 2.2.1.1 and 2.2.2.1.

The first step is to describe the forces measured by the accelerometers: their axes, xyz, coincide with the body frame axes and with the car coordinate system, and the relationship with the ENV coordinate system is described as follows:

$$\begin{bmatrix} f_{xb} \\ f_{yb} \\ f_{zb} \end{bmatrix} = R_G^b \begin{bmatrix} f_E \\ f_N \\ f_V \end{bmatrix} \quad (4.1)$$

Where R_G^b is the transformation matrix between the global frame (G) and the body frame (b) (Salytcheva, 2004). It follows that the forces describe the misalignment of the horizontal plane of the IMU and the horizontal plane of the global:

$$\begin{aligned} f_{xb} &= -g \sin \theta_y(\mathbf{0}) \\ f_{yb} &= g \sin \theta_x(\mathbf{0}) \end{aligned} \quad (4.2)$$

For small angles equation (4.2) can be rewritten:

$$\begin{aligned} f_{xb} &= -g \theta_y(\mathbf{0}) \\ f_{yb} &= g \theta_x(\mathbf{0}) \end{aligned} \quad (4.3)$$

This is shown in the following figure (Figure 4.1).

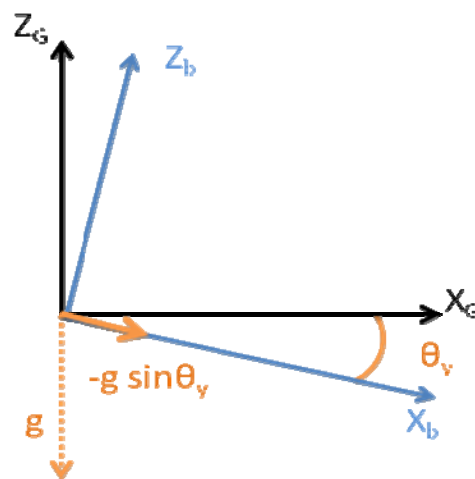


Figure 4.1 Horizontal misalignment between the body frame (b) and the global frame (G)

Now it is possible to estimate the angles θ_x and θ_y using the accelerometers' data: the first twenty seconds of measurements are used, since the car is standing still, it has to be found the average of these values and the result will be used to calculate the corresponding angles, using equations (4.2) or (4.3).

In this part of the project both angular velocities and Euler angles have been used in order to establish which method could be more convenient and more precise.

Considering the case of the angular velocities, derived from gyroscopes' measurements, the following steps have been performed: a bias has been estimated calculating the mean value of the first twenty seconds, then it has been removed just subtracting it from the data, these angular velocities have been integrated in order to obtain the corresponding angles, and finally from these resulting angles the initial misalignment angles calculated from the accelerations have been removed, to obtain measurements horizontally aligned and without biases.

In the case of using the Euler angles the procedure has been the same, just simplified since the data are already angles, hence there is no need to integrate.

The results of these two corrections are shown in Figure 4.2 for the X and Y axes.

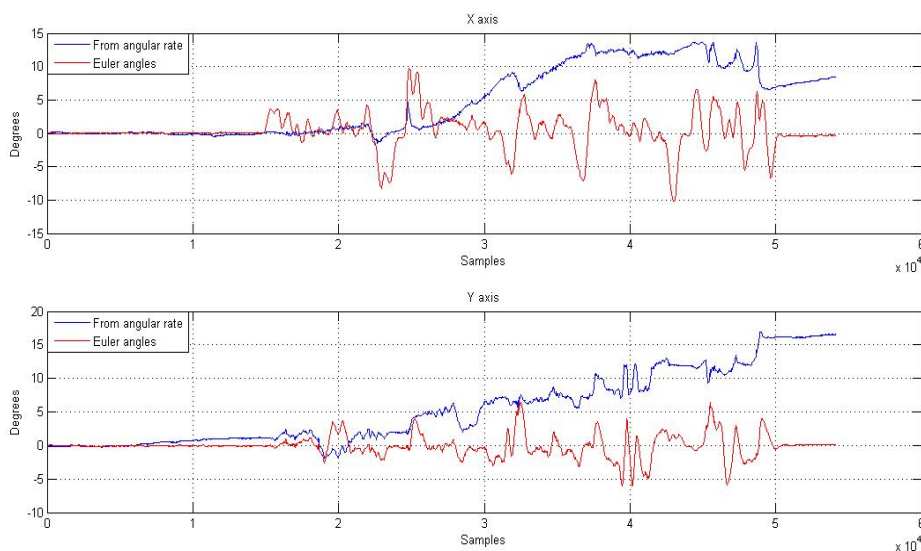


Figure 4.2 Angles derived from gyro measurements and Euler angles after correction

The blue line represents the resulting angles obtained with the angular rates, and the red line represents the resulting Euler angles. It can be noticed that for the angles obtained from the angular rates there is a very large drift, increasing really fast with time, which is mainly due to the integration of residual biases. From this graph the best choice would be to use Euler angles.

4.2.2 Removing of gravity components

The corrected angles obtained represent the initial misalignment of the IMU with the horizontal plane, and they have been used to remove the gravity components from the collected acceleration data as it has been previously explained. The results are shown in Figure 4.3 and Figure 4.4.

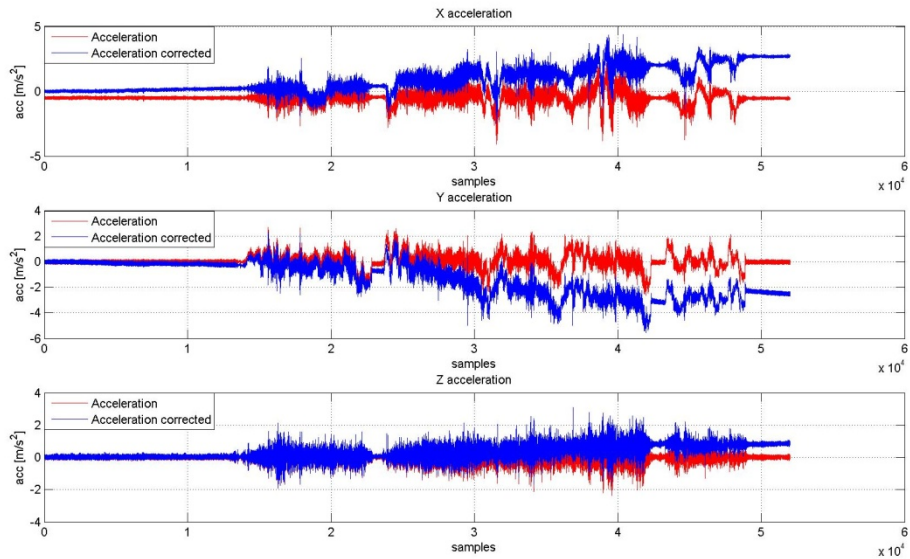


Figure 4.3 Removing of gravity components using the angles derived from the angular rates

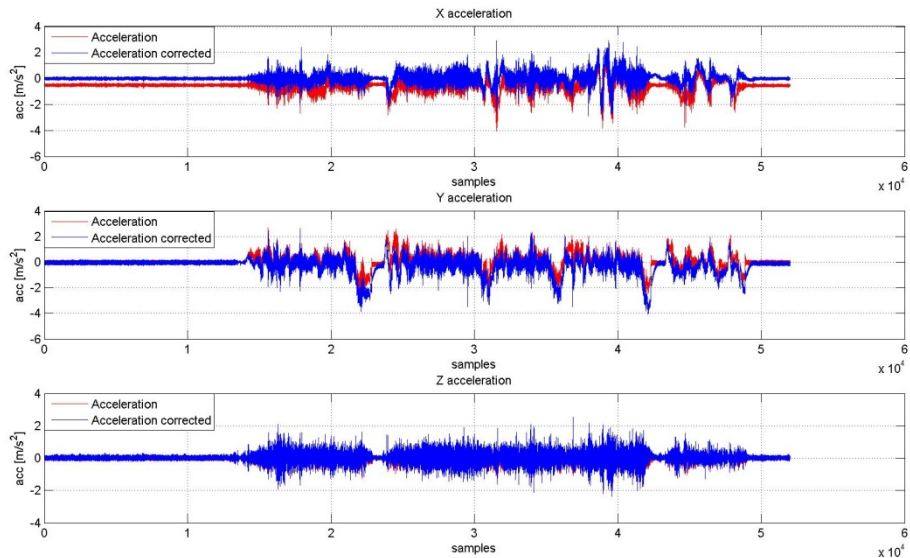


Figure 4.4 Removing of gravity components using the Euler angles

The figures above are both divided in three rows in which it is possible to observe the results obtained for X, Y and Z-accelerations: the red line represents the initial data, while the blue line represents the corrected data.

It can be noticed that using Euler angles the obtained results are better than those coming from the gyroscope measurements: one possible reason for this could be that the correction made is approximate since the removed bias was only calculated from the first 20 seconds, so in the angular velocities persist some biases and errors which, when integrated, give rise to a drift which increases very fast in time.

Nevertheless the Euler angles results are not good enough: as it can be seen in Figure 4.5, which is a zoom taken from the central plot of Figure 4.4, after the correction the accelerations look like there would be a delay in the sensor response: in fact the acceleration should be zero since the car is standing still, or at least the curves should result flat in that period of time, as the red ones do. One possible reason for this could be that some assumptions in the XKF are not fulfilled.

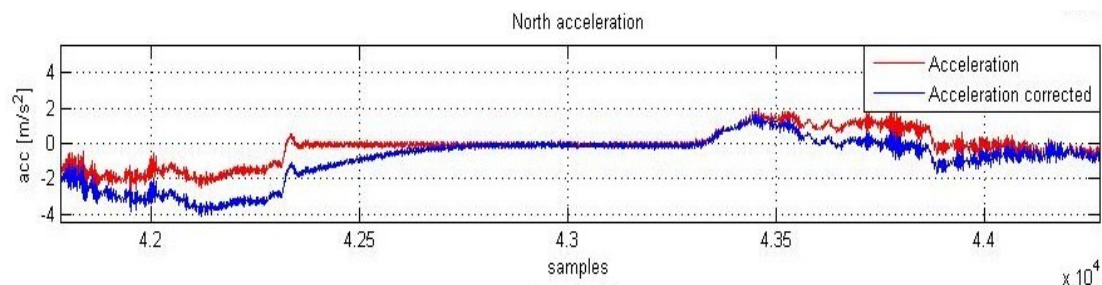


Figure 4.5 Zoom of the North acceleration compensation results

Because of the bad results obtained by removing the gravity components from the accelerations, with the two different techniques, it has been decided to not use this method, but to apply a simple bias removal using, as in the previous cases, the data collected in the first twenty seconds.

This solution gives as result a set of data not really precise and trustable, as it can be confirmed in section 5.1.2. Of course this fact influenced also the Kalman filter parameters, which have been set in such a way to not trust very much the accelerometers' measurements.

4.3 Synchronization

It has been illustrate in section 3.2 how the system was mounted in order to perform an automatic synchronization of the GPS and IMU measurements.

The procedure has been tested before the final experiment, though, when the collected data have been analyzed, it has been noticed that no external events have been marked in the RINEX file. It was not possible to identify the problem that occurred during the experiments.

An alternative solution to synchronize the data a posteriori is described in the following section.

4.3.1 Correlation

The correlation function describes a statistical relationship between two or more random variables or data.

The data related to the GPS are really similar to those related to the IMU, so, even if they cannot be completely identical it has to be possible to find a correlation between them. This can be used to synchronize the two signal, so they can be later used for the simulations.

The correlation has been calculated using the yaw rate data derived from the measurements with both navigation systems: this has been chosen because it is the most complex measurement, since the car was supposed to be always in the horizontal position, so the observable variations for the roll and pitch data should be small, while for the yaw rate should be bigger and more recognizable.

First of all the two data series have been plotted (see the upper subplot in Figure 4.6) in order to examine them and select two portions of data which seemed to be really similar: in this case a portion of 16000 samples, from sample 26000 to sample 42000, has been used. After that the correlation function “`xcorr`” has been applied to the data and set so that it would return a vector of lag indices and the correspondent correlation value: the lag related to the maximum correlation has been used to remove the delay from the IMU yaw rate.

To have a better estimate of this delay, this process has been repeated several times, using a Kalman filter, which principle of operation will be described in section 6, and giving as input just the GPS data: each time a multiplying factor used in the creation of the Q matrix, which contains process noise parameters used in the Kalman filter, has been increased to get a looser filter, and the GPS yaw rate recalculated. This operation was reducing the delay generated in the Kalman filter, but it was, in the same time, increasing the noise on the measurements. With the new yaw rate the lag for the maximum correlation was recalculated, and it was increasing at every round. When the multiplying factor reached the value of 10, a change in the GPS error setting has been necessary: in fact the error on the GPS measurements was changed from 2 m to 1 m, in order to reduce the noise in the filter, which was getting too large. The estimation has been performed until a good compromise between the noise and the delay has been found, and the lag value has been considered stable and maximum. The final estimation of the delay of the IMU data was of 784 samples, which corresponds to 7.84 seconds. This has been finally removed from the IMU data, and both functions have been plotted again together to observe the results (see the lower subplot in Figure 4.6).

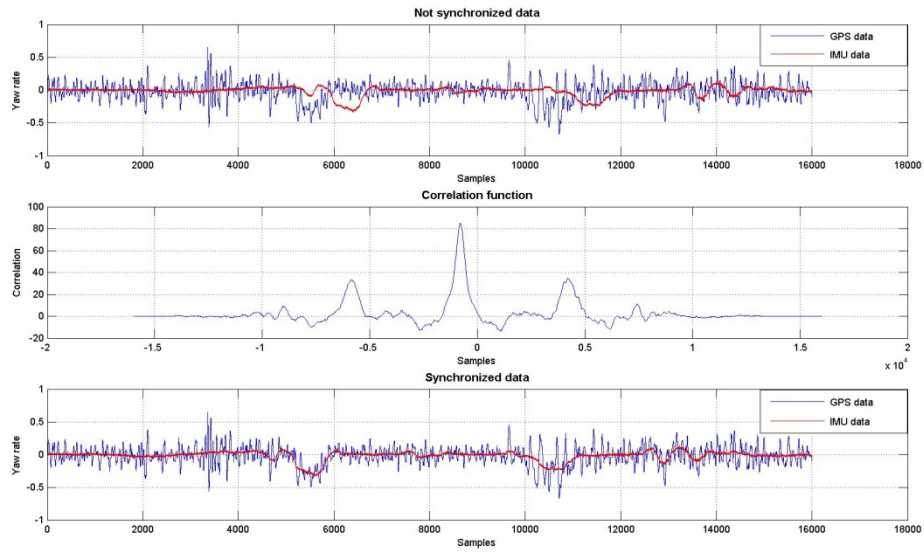


Figure 4.6 GPS and IMU yaw rate before the synchronization; resulting correlation function; GPS and IMU yaw rate after the synchronization.

It can be seen, in the upper plot in Figure 4.6, a similarity in the GPS data curve (blue line) and the IMU data curve (red line), which has been used for calculating the correlation function.

5 Measurement's noise estimation

As it has been explained in sections 2.2.1.1 and 2.2.2.1, IMU measurements are affected by some noise processes. In order to describe some properties of these processes two techniques have been used in this project, and they are presented in this chapter, followed by the results for both gyroscopes' and accelerometers' data.

The first technique used is the standard deviation, which measures the variability of the data, and the second is the Allan deviation, which is actually the standard deviation just applied in a special case.

It has to be noticed that both analysis have been static ones, so they have been performed using data collected when the car was standing.

5.1 Standard deviation

Before explaining the concept of standard deviation, the idea of variance has to be introduced. In probability theory and statistics, the variance is used as one of the several descriptors of a distribution (Wikipedia - Variance, 2010): it illustrates the behaviour of the data set indicating how different the values are from the mean value and, in case of a discrete random variable X , with probability mass function $x_n \rightarrow p_n$, it is calculated as follows:

$$\text{Var}(X) = \sum_{i=1}^n p_i \cdot (x_i - \mu)^2 \quad (5.1)$$

where

$$\mu = \sum_{i=1}^n p_i \cdot x_i$$

The standard deviation is defined as the square root of the variance and it gives a measure of the variability or dispersion of the data. When the standard deviation is large it means that the values contained in the data set are spread over a large range of values, far from the mean value, while if it is small it means that the values tend to be close to the mean.

This expression is much more used and useful than the variance since it is expressed with the same unit of the analysed data.

To estimate the standard deviation of the gyroscopes' and accelerometers' measurements, data collected in the first thirty seconds have been used, in order to have a more stable mean value, since the car was standing still.

5.1.1 Gyroscopes' data

In this section the results of the calculations are presented, and compared with the performance specifications furnished by the producer of the MTi. The data are all referred to the first thirty seconds of measurements, done with a sample rate of 100 Hz.

In Xsens manual it is possible to find out that the noise density for the turn rate is $0.05 \frac{\text{units}}{\sqrt{\text{Hz}}}$, which means, having a bandwidth of 100 Hz, that this noise density has to be multiplied by a factor of 10.

Table 5.1 Standard deviation of gyroscopes' data

Parameter	Value	Units
Standard deviation X axis	0.34	deg/s
Standard deviation Y axis	0.34	deg/s
Standard deviation Z axis	0.31	deg/s
Noise density given by Xsens	0.5	deg/s

It can be noticed from the table that the results got with the experimental measurements are better than expected. This could be due to the conditions in which the experiments have been conducted, which could be particularly convenient, or it could just be a not precise measurement since the data refer to a period of time very short, which cannot really be considered a good reference. It is also important to notice that the acquisition system has been subject of the vibrations of the car engine during the driving test, and these vibrations have not been removed from the data used for the noise classification.

5.1.2 Accelerometers' data

In this section the results of the calculations are presented, and compared with the performance specifications furnished by the producer of the MTi. As in the previous paragraph the data are referred to the first thirty seconds of measurement and the sample rate used is 100 Hz.

Table 5.2 Standard deviation of accelerometers' data

Parameter	Value	Units
Standard deviation X axis	0.0658	m/s ²
Standard deviation Y axis	0.1002	m/s ²
Standard deviation Z axis	0.1032	m/s ²
Noise density given by Xsens	0.02	m/s ²

In this case the results obtained are worse than the specification given by the producer: it is probably due to the short length of the data sequence.

5.2 Allan deviation

The Allan deviation is based on a variance as the standard deviation.

The Allan variance (AVAR) is also known as the two-sample variance, it is a function of averaging time and it is the most common time domain measure of the frequency stability of a device. It is calculated as follows:

$$AVAR(\tau) = \frac{1}{2 \cdot (n-1)} \sum_i (a(\tau)_{i+1} - a(\tau)_i)^2 \quad (5.2)$$

Where $a(\tau)_1 \dots a(\tau)_n$ are averages on the averaging time τ , and where n is the number of bins in which the data sequence is divided into (Woodman, 2007).

Similar to the standard variance, it is a measure of the fractional frequency fluctuations, but it has the advantage of being convergent for most types of clock noises (Riley, 2008).

The Allan deviation is defined as the root square of the Allan variance, and it is used to characterize noise processes. In order to do this it is usually plotted on a log-log scale to be able to compare the results with the graph shown in Figure 5.1. Different types of random processes cause slopes with different gradients to appear on the plots, furthermore different processes usually appear in different regions of τ , allowing their presence to be easily identified (Woodman, 2007).

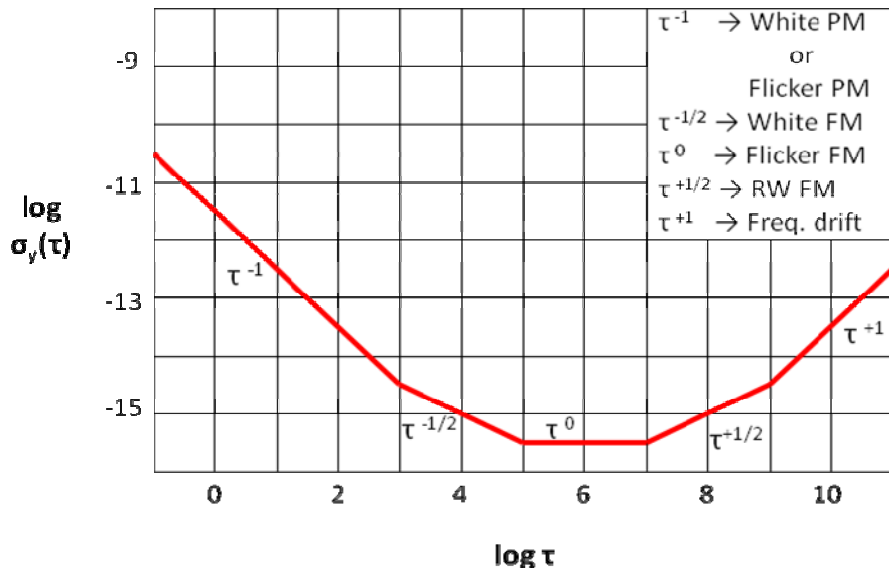


Figure 5.1 Sigma-tau diagram, Allan deviation

There are many adaptations of the Allan variance method, such as the overlapping Allan variance and the modified Allan variance. The first one makes use of all the

possible combination of the data set, as shown in Figure 5.2, which means that the results are more reliable, since the effective number of degrees of freedom is increased, but it needs a larger computational time.

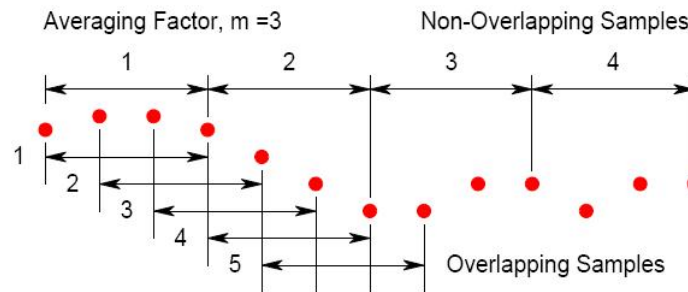


Figure 5.2 Comparison between non-overlapping and overlapping methods

However the most useful is the modified Allan variance: it is the same as the normal Allan variance for $n = 1$, but it includes an additional phase averaging operation and it has the advantage of being able to distinguish between white and flicker PM noise (Riley, 2008).

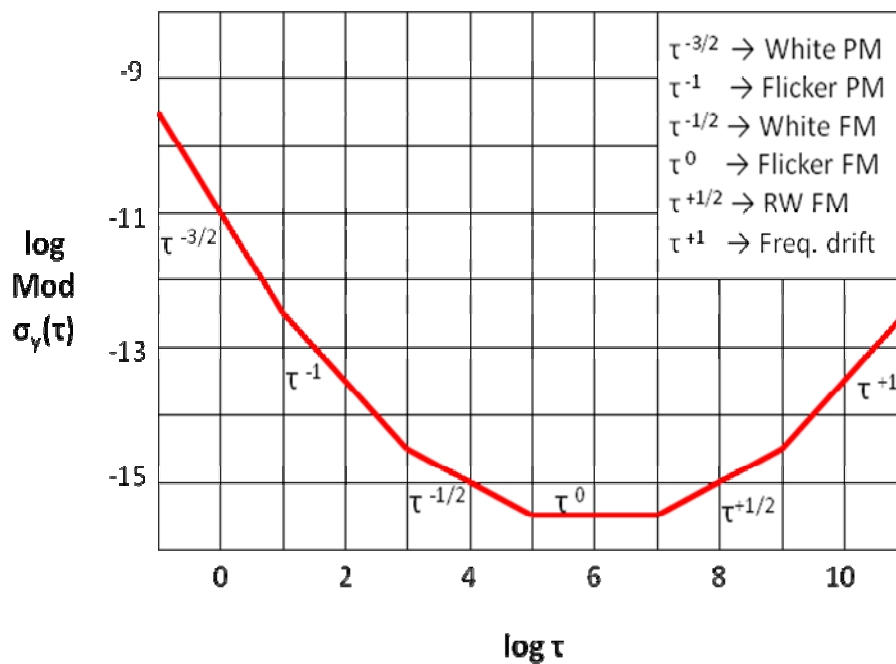


Figure 5.3 Mod sigma-tau diagram, modified Allan deviation

5.2.1 Gyroscopes' data

In this section the plots obtained are shown and analyzed to determine the dominant noise process. Data sequences of 10000 samples, that is 100 seconds, are used at the usual sample rate of 100 Hz.

In the plots that follow just the overlapping (blue line) and modified (red line) variance methods are shown, because the normal Allan deviation's results are too unstable to make possible the identification of the slope of the resulting curve. This is mainly due to the fact that the period of time used is really too short to have a precise and trustable frequency stability analysis.

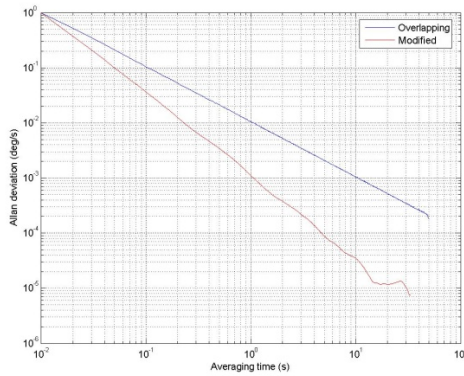


Figure 5.4 Allan deviation, X axis

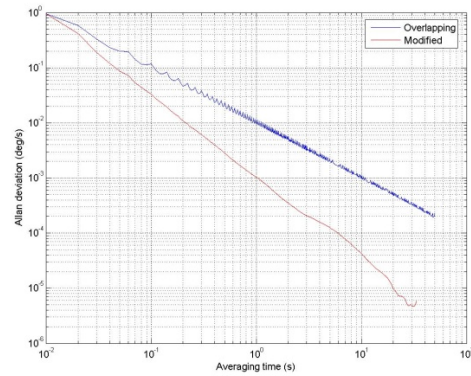


Figure 5.5 Allan deviation, Y axis

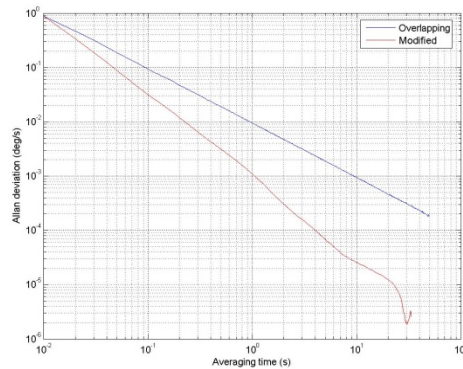


Figure 5.6 Allan deviation, Z axis

It can be noticed that for the slope of the overlapping Allan deviation is approximately -1, which, referring to Figure 5.1, reveals the presence of white or flicker noise in the measurements. Checking the modified Allan deviation curve, with slope of -3/2, it can be determined that it is white noise.

5.2.2 Accelerometers' data

In this section the plots obtained are shown and analyzed to determine the dominant noise process. Data sequences of 10000 samples, that is 100 seconds, are used at the usual sample rate of 100 Hz.

As in the previous case just overlapping and modified Allan variance methods are shown.

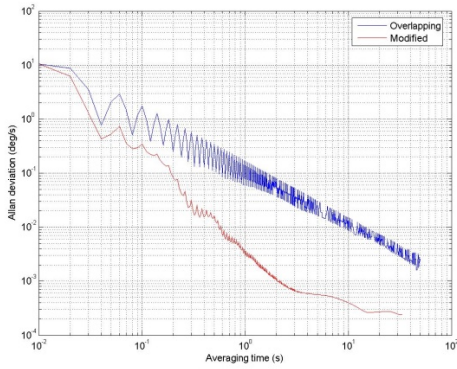


Figure 5.7 Allan deviation, X axis

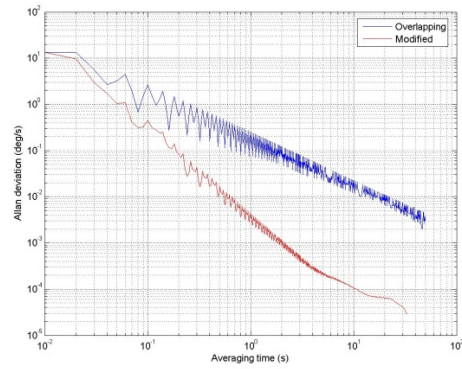


Figure 5.8 Allan deviation, Y axis

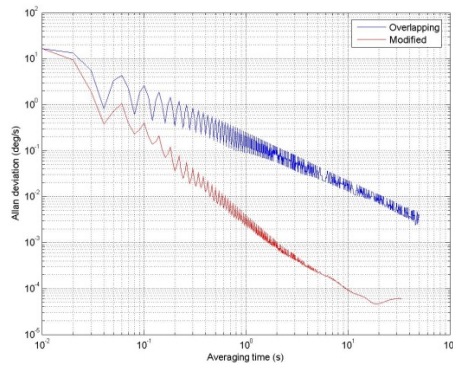


Figure 5.9 Allan deviation, Z axis

In this case the resulting curves are more inconstant, especially in the first part of the plot, but their general behaviour is the same that has been obtained with the gyroscopes' measurements: the overlapping Allan deviation shows that there is white of flicker noise, and the overlapping method confirms that it is white noise.

So the conclusion is that the collected data are affected by white noise for both sensors.

6 Simulations

In this section is going to be explained how the simulations have been run: first of all the available data are presented, in order to know which is the starting point of the simulation. It follows a description of the generated data used as inputs for the Kalman filter, and of the different scenarios which have been simulated. In the end the modeling part of the simulations is described, followed by the Kalman filter inputs and outputs.

6.1 Available Data

In the following table the available measurements are described: these are the data that were collected during the experiments and which have been processed as previously described.

Table 6.1 Available Measurements

Available Measurements		Sample Rate	Measurement uncertainty (σ)
GPS	Code position	20 Hz	~1 m
	Phase position	20 Hz	~1cm
IMU	Acceleration	100 Hz	~0.09 m/s ²
	Angular rate	100 Hz	~0.33 deg/s

6.2 Generated Data

In the following table the generated data are described. These are the data which have been used as input for the Kalman filter in the simulations.

First of all it has been necessary to evaluate the position of the vehicle through the GPS code data collected, and in this case a sample rate of 1 Hz have been considered: this choice was due to the fact that the GPS receiver used for this project was a professional one, while the common ones usually work with a frequency of 1 Hz.

Then, as it was already mentioned, it has been necessary to generate RFID and CAN measurements: these were based on GPS phase measurements, which means that the sample rate was of 20 Hz and that the measurement uncertainty was 1 cm. Nevertheless it has been considered that the RFID points have been collected with a certain frequency (in this case the same of the GPS receiver) and then just some of them have been inserted in the simulations.

Table 6.2 *Generated data, used as input to the Kalman filter, and their origin*

Generated data...		Sample rate	Measurement uncertainty (σ)	...their origin
GPS	Position	1 Hz	~1 m	GPS code data
IMU	Acceleration	100 Hz	~0.09 m/s ²	IMU measurements
	Angular rate	100 Hz	~0.33 deg/s	IMU measurements
RFID	Position	20 Hz	~1cm	GPS phase data
CAN	Speed	20 Hz	~1cm	GPS phase data

In order to analyze the performances of the system when no GPS satellites are visible, some GPS outages have to be inserted in the simulation, so different scenarios have to be tried.

Two different situations have been considered: GPS outages without having RFID points, and GPS outages having RFID points. It has been decided to use four points and they have been spread in the data set to observe the effect of having them in the listed situations. In the case of having the RFID points the measurement noise value used is of 0.5 m, and the reasons for choosing this value are explained in section 6.3. The points have been placed in the epochs number 3040, 5400, 7424 and 8660 (out of a total of 10400 epochs).

For the simulation the data set has been cut in order to have 520 seconds of measurements, that means 8 minutes and 40 seconds: in this way the last twenty seconds of measurement, in which the car is standing, are not considered but the numbers used are easy to understand and use, in fact working with sources with different sample frequencies the calculations become much easier having a round number of samples.

In the following table the different scenarios are listed.

Table 6.3 Scenarios used for the simulations

Scenario code	RFID	GPS outages (from second n° to second n°)
1.1	No	230→315
1.2	No	180→250; 320→400
1.3	No	180→230; 270→330; 390→460
2.1	Yes	230→315
2.2	Yes	180→250; 320→400
2.3	Yes	180→230; 270→330; 390→460

6.3 Modeling

In a real case it would have not been possible to control the Kalman filter inputs in real time, but since in this case it has been performed a simulation, some parameters have been changed to observe the final results and to find what could be the best solution for different situations. Anyway in this section are considered only the parameters that could actually be changed in a real case.

In the following table the measurement used by the Kalman filter are listed.

Table 6.4 Kalman filter measurement modeling

Measurement Type		Measurement uncertainty (1σ)
Position	GPS	1 [m]
	RFID	0.5 [m]
Acceleration	IMU	2 [m/s ²]
Angular rate	IMU	0.03 [rad/s]
Speed	CAN	0.2 [m/s]

It can be noticed that the measurement uncertainties are different from those listed in Table 6.: this because it has been possible to set them through the simulation software. It has to be specified that they are not related to the real measurements, since they refer to the noise of the GPS data. What has been done was just to modify the noise

parameters in the Kalman filter in order to trust these data more or less when it would be time to merge them.

For example for the acceleration data coming from the IMU measurements, the uncertainty of the collected data was around 0.09 m/s^2 , but since it has not been possible to perform the gravity compensation, it is reasonable to assume that the Kalman filter should not trust these measurements as much as the angular rates, which do not need any particular compensation or correction.

In the case of the RFID points it could have been used a value of 1 cm, which was the measurement noise on the generated RFID data (coming from the GPS data with the same precision), but it has been set a measurement uncertainty of 0.05 m since this value could be a more realistic one. The RFID points could help anyway to recover the right position, but it was interesting to see how big influence can this higher uncertainty have on the final result.

In the following table the Kalman filter state modeling is summarized.

Table 6.5 Kalman filter state modeling

State variable name	Description	Process noise (1σ)
East Position	East Position of vehicle in local ENV coordinate system	-
North Position	North Position of vehicle in local ENV coordinate system	-
Speed	Speed of vehicle in forward direction	-
East Acceleration	Acceleration of vehicle in east direction	0.05 m/s^2
North Acceleration	Acceleration of vehicle in north direction	0.05 m/s^2
Direction Angle	Angle of vehicle, measured clockwise from north axis in the local horizontal plane (ENV coordinate system)	-
Angular rate	Rate of change of vehicle direction angle	$\pi/90 \text{ rad/s}$

6.4 Kalman outputs

In this section the software used for the simulations is going to be analyzed giving a brief description of the outputs of the Kalman filter. The plots of the outputs will be shown in section 7.

With all the information about the inputs, given in sections 6.2 and 6.3, the simulations have been run and the outputs that have been obtained are mainly observable through the plots described in section 7: they show the horizontal position calculated by the Kalman filter, as a result of the four data sources, plotting also the resulting errors in form of error bars. These plots are useful to analyze the different scenarios, which are presented in the following section.

Other outputs that are given from this simulation are the azimuth angle of the car, the yaw rate expressed in radians per seconds, the horizontal speed, the east acceleration and the north acceleration.

7 Results and comments

In this section the results of the simulations are presented and commented, followed by an error analysis where the Kalman filter expanded measurement uncertainty is studied, and the position is assessed using the GPS phase position as a true position.

Regarding the results just the horizontal position is analyzed since it contains all the other information, and also because it is the most intuitive plot: in fact it shows if the MTi can be useful, and if so, up until what level, for tracking the position of a vehicle when there are GPS outages.

7.1 Horizontal position

Horizontal position plots have been really useful, especially to see how close the measurements are to the real path shown in Figure 3.1. Nevertheless it has been noticed that no big differences can be observed with this kind of plots, when different scenarios are compared. In fact the differences can be efficiently pointed out in the error plots, presented in next section.

First of all the scenarios without RFID points are analyzed for the three different GPS outages. In the following plots the blue dotted line represents the GPS input for the Kalman filter: it means that it shows the position we would have had if only GPS was used. The green line represents the output of the Kalman filter, which is the resulting position we get from the sensor fusion.

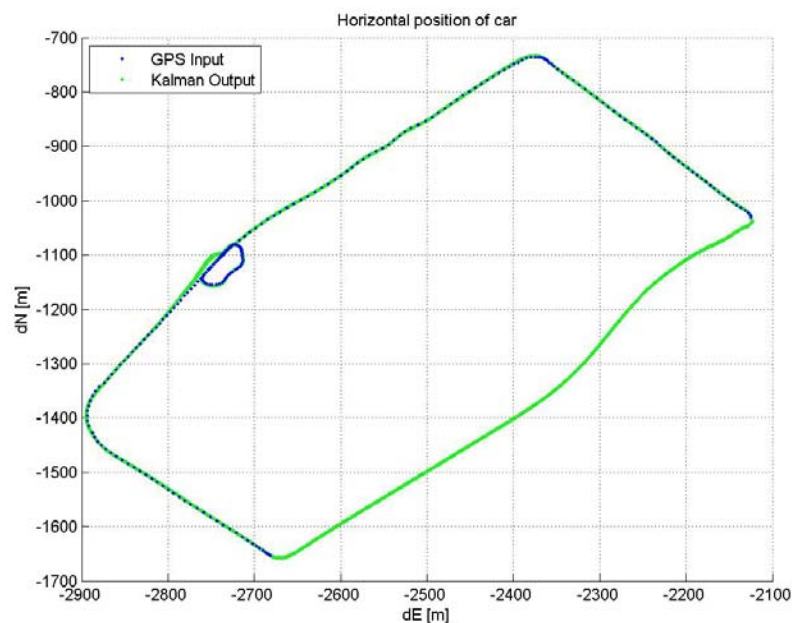


Figure 7.1 Horizontal position, scenario 1.1

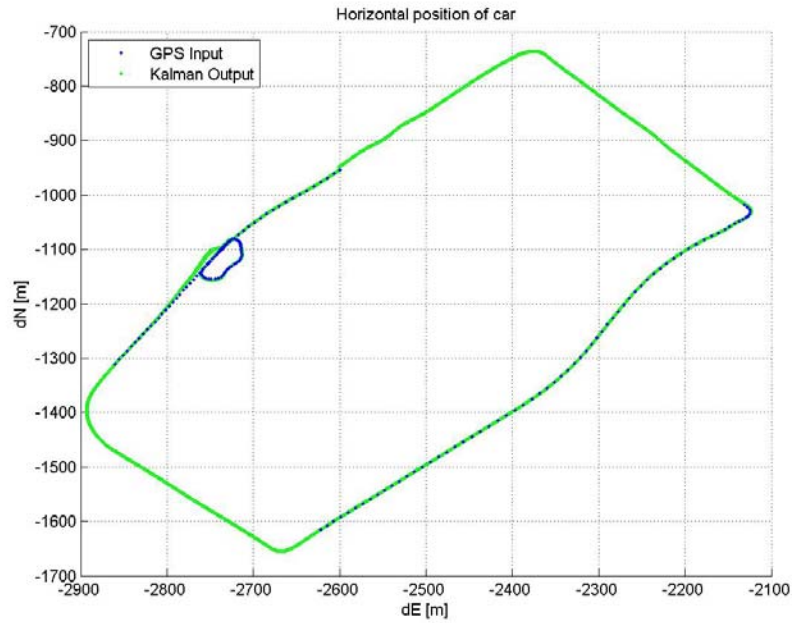


Figure 7.2 Horizontal position, scenario 1.2

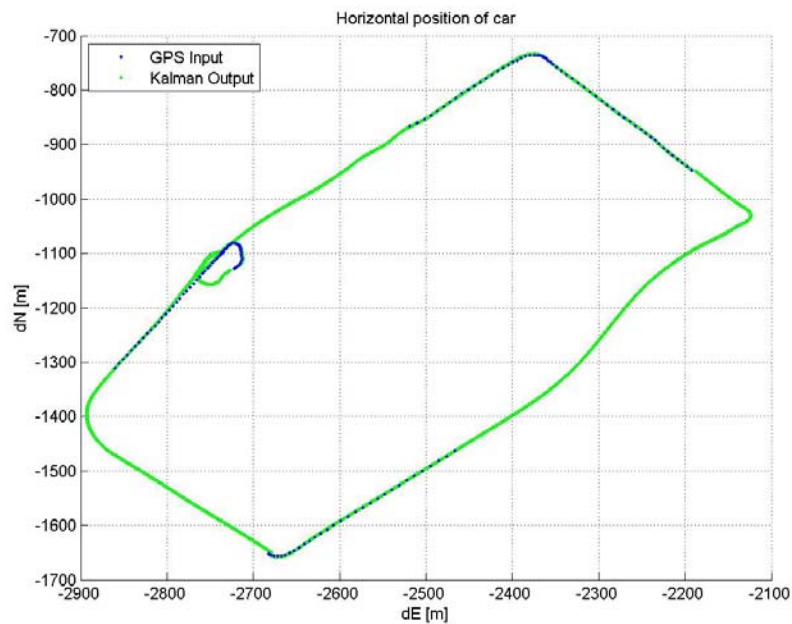


Figure 7.3 Horizontal position, scenario 1.3

The blue dots show, in a more intuitive way than the Table 6.3, the periods of time, over the path, when we have GPS data, and the remaining green line shows the GPS outages.

It can be noticed that at the end of every GPS outage the signal 'jumps' back to the more reliable value given by the GPS measurements, and in this way it is possible to estimate if a big drift has been developed (the distance between the last outage point

and the first GPS point is large) or not. In the following figures this can be better observed:

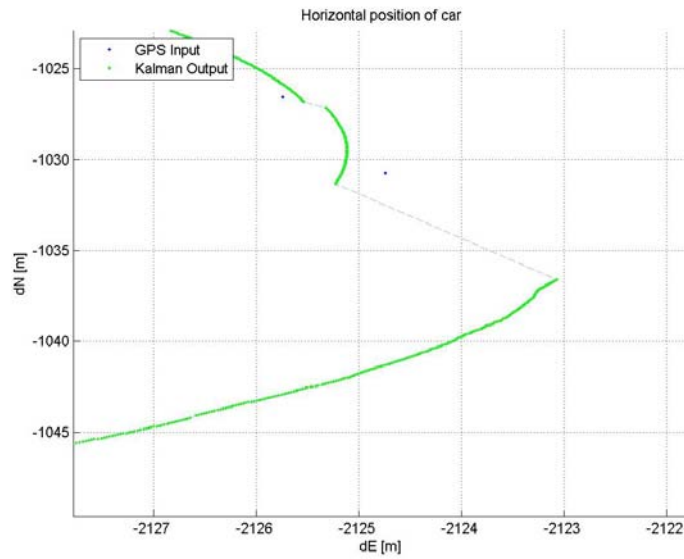


Figure 7.4 Zoom of horizontal position, scenario 1.1

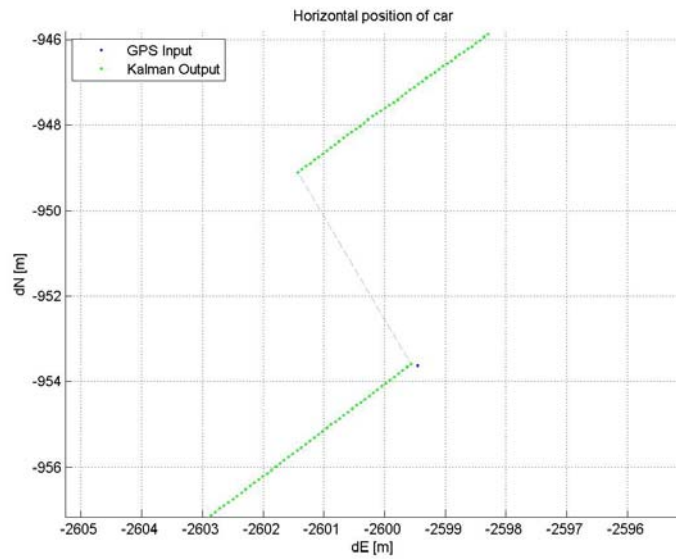


Figure 7.5 Zoom of horizontal position, scenario 1.2

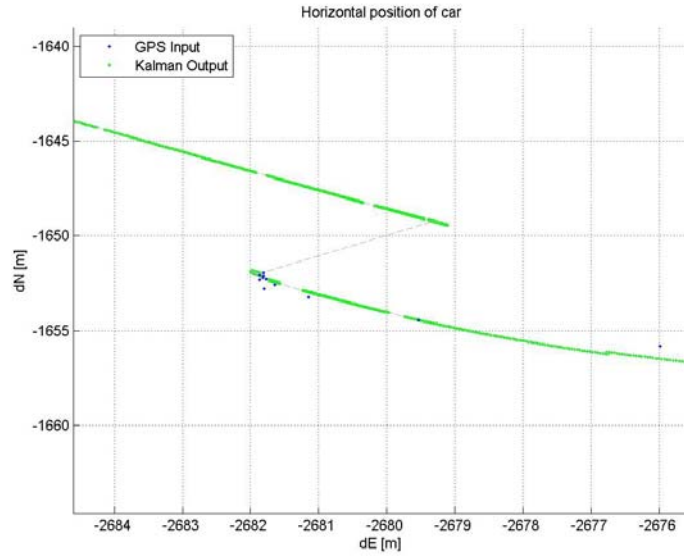


Figure 7.6 Zoom of horizontal position, scenario 1.3

The following group of plots is referred to the second scenario with RFID points and with measurement noise of these points equal to 0.5 m.

In this case it is possible to recognize that the RFID points reduce the drift of the output during GPS outages: the output estimate gets the corrections and the total error is much less than in the previous case. This will be shown better in section 7.2.

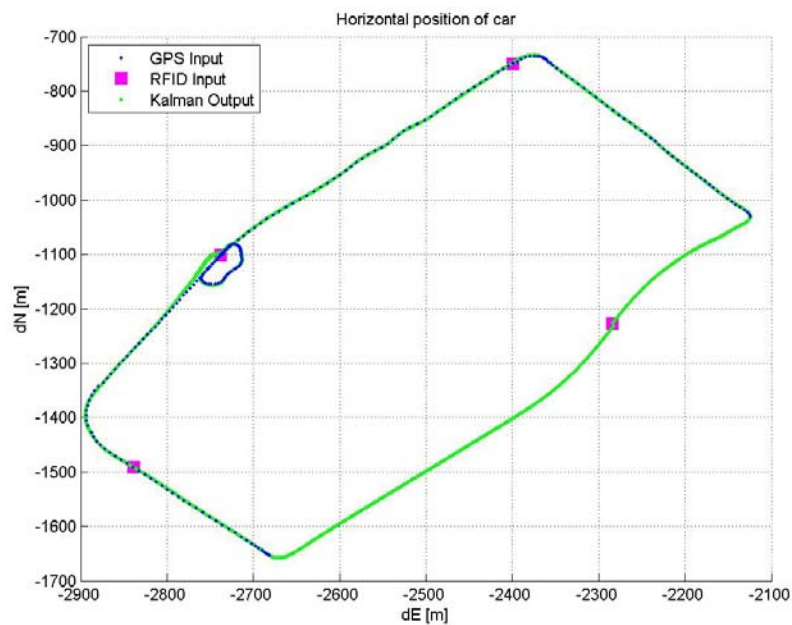


Figure 7.7 Horizontal position, scenario 2.1

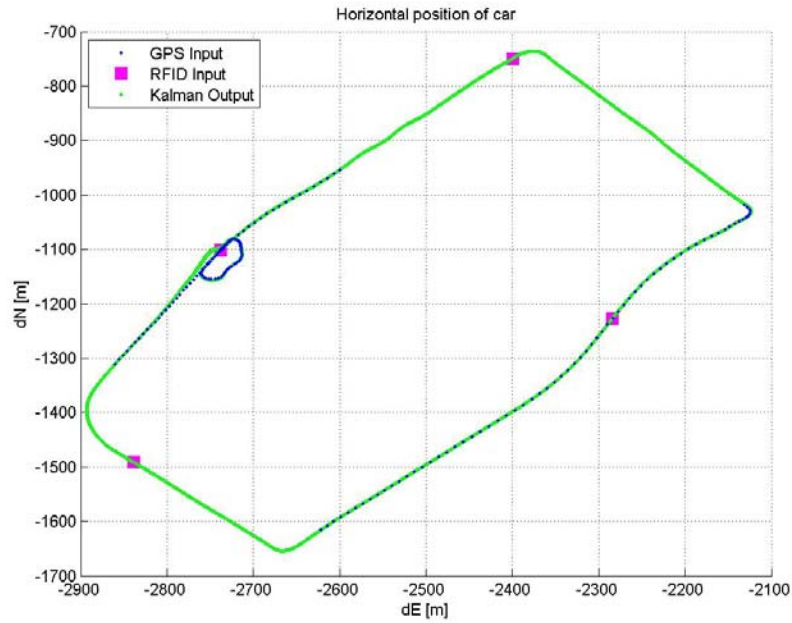


Figure 7.8 Horizontal position, scenario 2.2

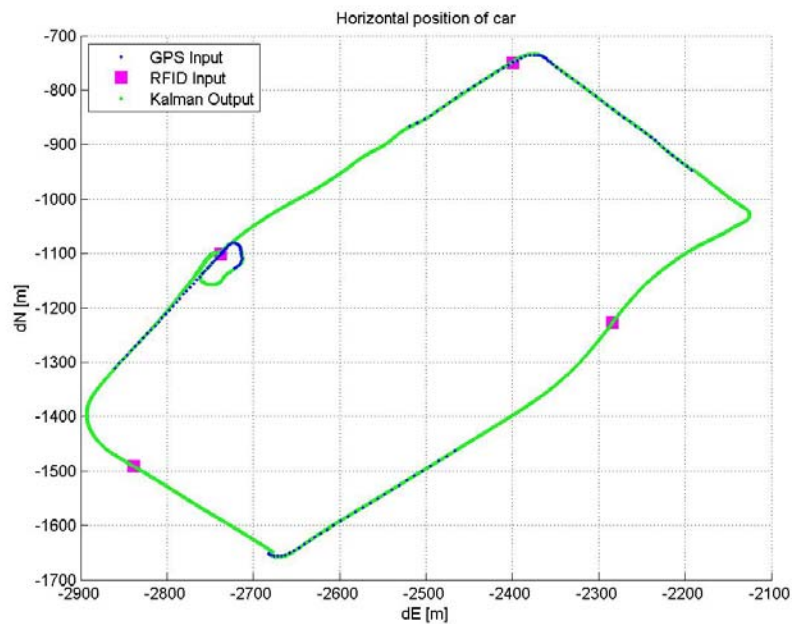


Figure 7.9 Horizontal position, scenario 2.3

It has already mentioned that the RFID points have been spread all over the path, and in these plots this can be observed. They help to reduce the drift when they are in the middle of a GPS outage, or they add precision to the system when inserted in the Kalman filter in a region which already has GPS data.

As it can easily be noticed, all the plots shown until now describe perfectly the path where the experiment was run, which means that the positioning system works quite well in different conditions.

7.2 Errors

In this section the errors related to the previous scenarios' results are shown and commented.

In the following graphs the red vertical bars represent the Kalman filter expanded measurement uncertainty, the black line represents the difference between the estimated position and the GPS phase position, assumed to be the true position, finally the blue line points out the GPS outages, to better understand the results.

In the upper graph it is shown the East position error while in the lower graph there is the North position error.

As it has been said, the first scenario does not include any RFID point, so the errors in the three different GPS outage combinations are the following:

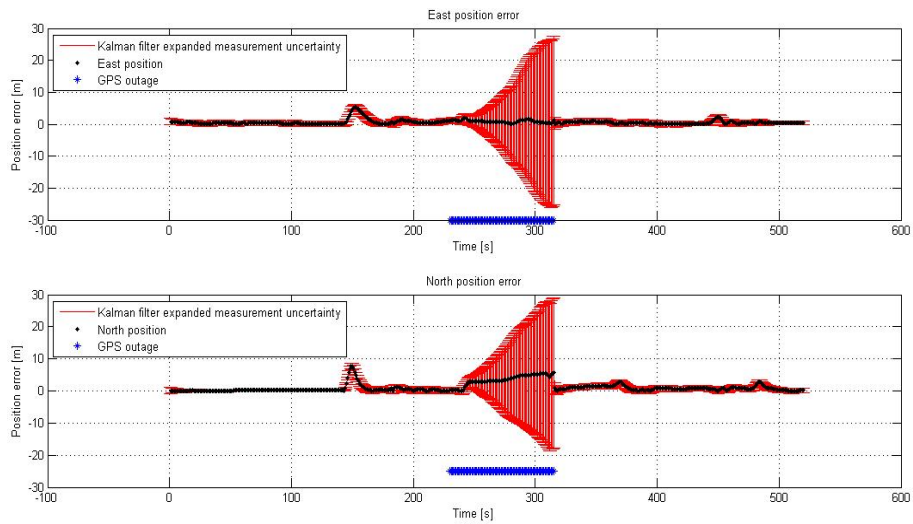


Figure 7.10 East and north position errors, scenario 1.1

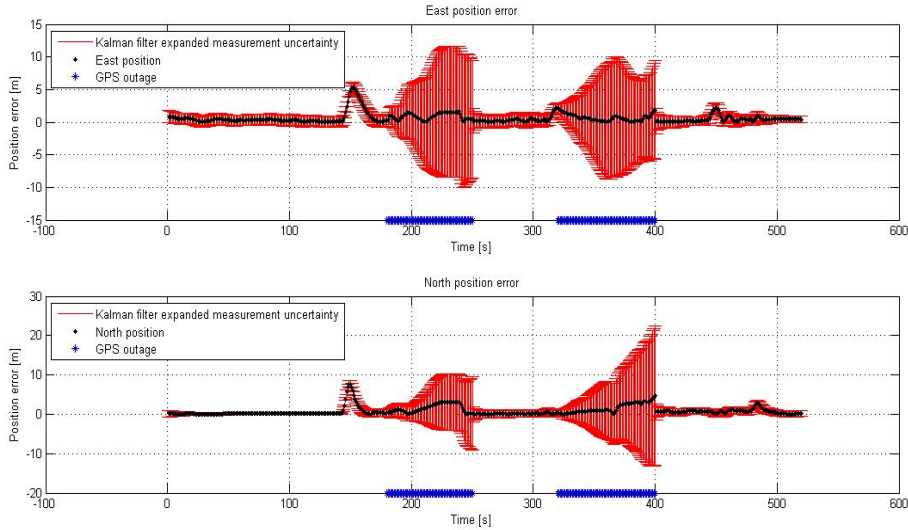


Figure 7.11 East and north position errors, scenario 1.2

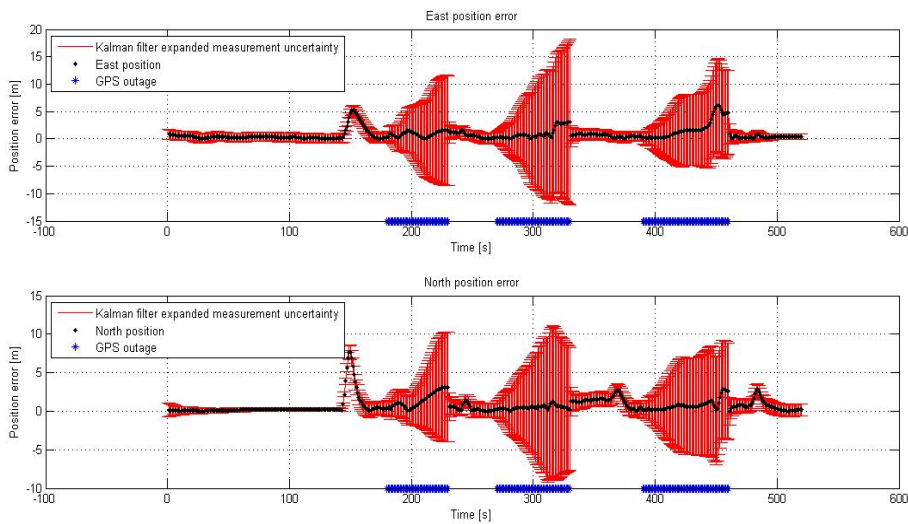


Figure 7.12 East and north position errors, scenario 1.3

In these figures it is possible to observe the drift of the calculated position when GPS data are not available. The uncertainty grows really fast in time, even if the estimated position still follows the correct path. The errors considered here to plot the error bars are 2σ errors, so we have the 95% of probability that our measurements are in the range shown by the bars.

The second scenario includes the RFID points with a measurement noise of 0.5 m, plotted as green dots on the same line where the GPS outage is shown.

With this scenario the improvement introduced by the RFID measurements is really obvious: whenever one point is in correspondence of a GPS outage, it reduces drastically the uncertainty, bringing the position error back to zero (or almost zero) as the outage had just started. This reduces the drift and stabilize the measurement.

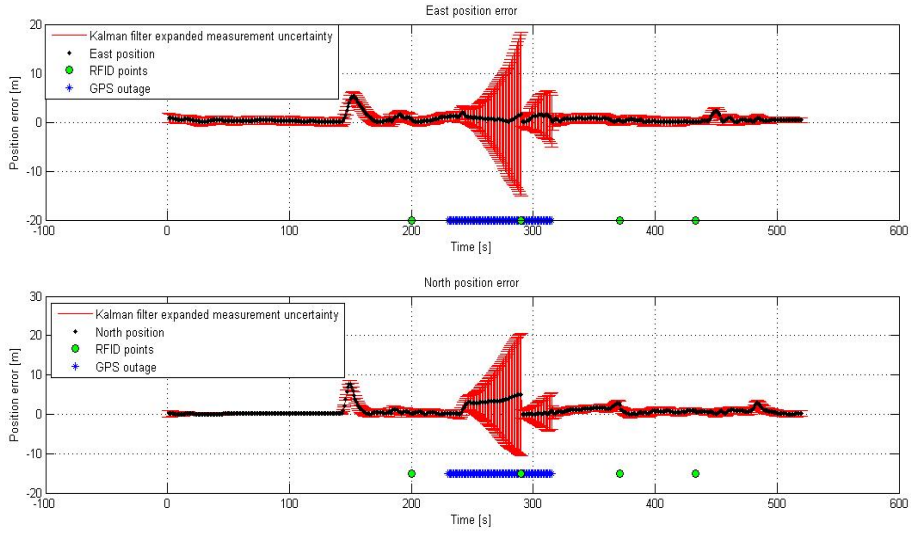


Figure 7.13 East and north position errors, scenario 2.1

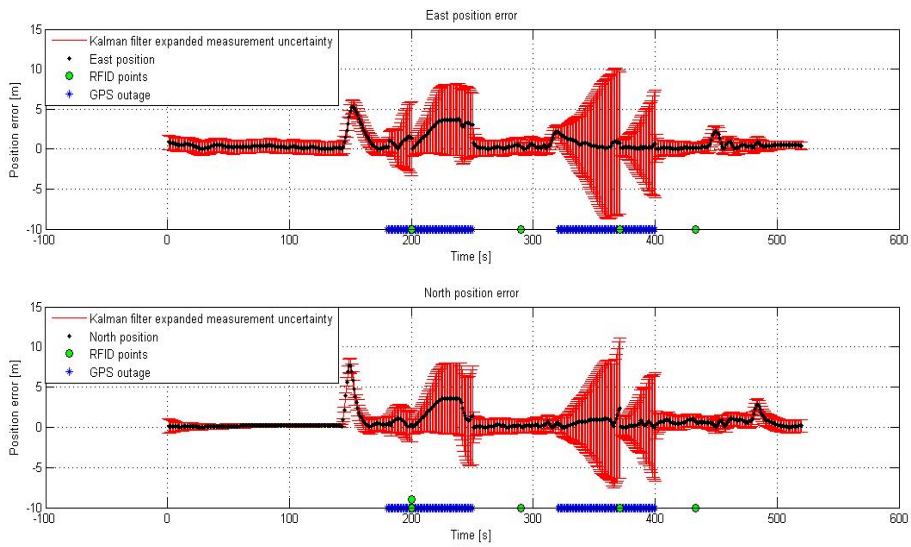


Figure 7.14 East and north position errors, scenario 2.2

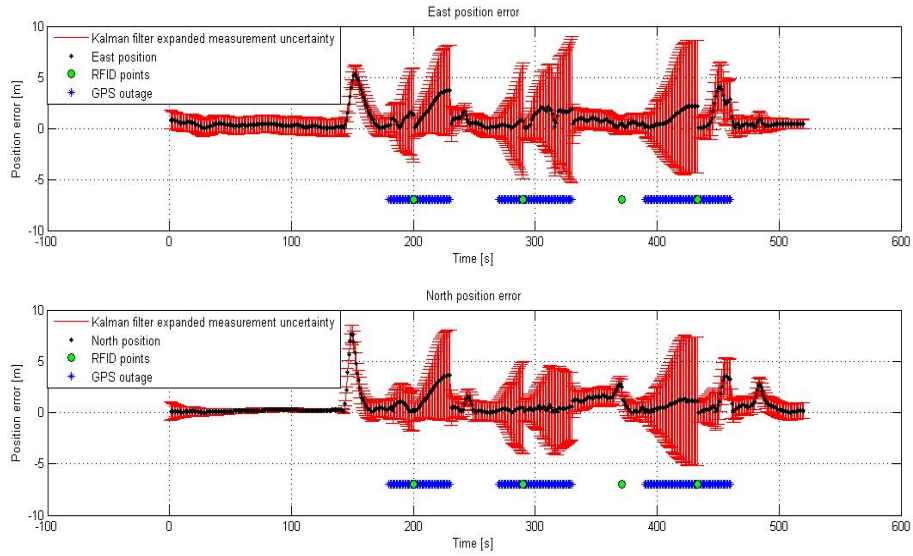


Figure 7.15 East and north position errors, scenario 2.3

What can be concluded is that even if the measurement noise for the RFID gets larger than the one referred to the GPS measurements, its help is visible in the tracking process and the resulting position error related to it grows in a smaller extent, compared to the first scenario.

In the following table some numerical results can be observed: in fact it is performed a comparison between the maximum expanded measurement uncertainties for the different scenarios.

Table 7.1 Maximum expanded measurement uncertainties for the different scenarios

Scenario	Without RFID		With RFID (0.5 m)	
	East	North	East	North
1	± 27 [m]	± 24 [m]	± 16 [m]	± 10 [m]
2	± 18 [m]	± 16 [m]	± 7 [m]	± 7 [m]
3	± 16 [m]	± 15 [m]	± 8 [m]	± 7 [m]

It has always to be considered that it is used a 2σ error, which means that it is really large: in fact it was observed that the results are really similar to the path actually performed.

8 Discussion and conclusion

8.1 Discussion

The results saw in the previous section showed the improvements reached with the sensor fusion including the RFID points: for example having a long period of GPS outage the maximum expanded measurement uncertainty is between 24 and 27 m, but with the sensor fusion this stays between 10 and 14 m. Nevertheless there are many aspects in the project that could be improved.

A first one is the synchronization of the data: it could be useful for future applications to find a reliable and automatic solution for the synchronization of the IMU with the GPS incoming data.

Another aspect that can definitely be improved is the horizontal alignment and error compensation of the system: first of all it could be found a more stable and cushioning way to mount the receivers on the car, in order to reduce vibrations and get more constant data, especially when the car is standing. This could improve the initial bias compensation making it much more efficient, also it would reduce the need to apply an error compensation on the collected data: in fact for this project it has been considered that the car has been driving in horizontal position, but the initial gravity compensation described in section 4.1 eventually did not work properly. It could be interesting to have a perfectly horizontal driving test, and analyze the results. It could be also important to study more in details the noise characteristics, to try to make a model for a better compensation. Finally it could be good to have even better performance gyroscopes, so their drift would be smaller and the gravity compensation could probably reach better results.

In the Kalman filter the accelerometers' measurements were not trusted very much because of the problems with the gravity compensation, so instead of them the most trusted data used for the positioning during GPS outages have been angular rates, from gyroscopes, and speed measurements. It came out that this could be a good alternative to avoid the problem with gravity compensation that arises in a low-cost IMU.

For a professional measurement's noise estimation of the IMU it would be good to execute a long static survey: in fact, for a reliable Allan deviation estimation, data should be collected for at least 12 hours. And obviously a dynamic analysis could also be of big interest.

8.2 Conclusion

The system assembled showed how a simple, but fully functional, sensor fusion can be realized with a low-cost device.

This sensor fusion system provides the position of the vehicle it is mounted on, data useful to analyse the acceleration and the speed of the vehicle itself, and many information about the errors which affect the whole project.

The Kalman filter could perfectly match data coming from two very different devices, based on different criteria and with different resolution, and this clearly indicate that with the improvements suggested in the previous section, higher performances could be reached.

An aspect that cannot be ignored is that the generated data used have a really high precision, which gives better data than what could be expected in reality. A future work could include another step in the project which consists in adding some noise to the RFID and CAN measurements, to make them more realistic.

In the end it can be said that this system represents a good starting point for a future development of low-cost “assistance” for the well known GPS receivers.

9 References

- Barbour, N. M., Elwell, J. M., & Setterlund, R. H. (1992). *Inertial instruments: where to now?* Cambridge, Massachussets.
- Grewal, M. S., Weill, L. R., & Andrews, A. P. (2007). *Global Positioning Systems, Inertial Navigation, and Itegration - Second edition*. Wiley.
- Hofmann-Wellenhof, B., Lichtenegger, H., & Collins, J. (2001). *Global Positioning System. Theory and Practice*. Wien.
- Kreye, C., Eissfeller, B., & Ameres, G. *Architectures of GNSS/INS Integrations - Theoretical Approach and Practical Tests -*. Munich, Germany.
- Riley, W. J. (2008, July). Handbook of frequency stability analysis. *NIST Special Publication 1065* .
- Salytcheva, A. O. (2004). *Medium Accuracy INS/GPS Integration in Various GPS Environments*. Calgary.
- Stovall, S. H. (1997). *Basic Inertial Navigation*. Navigation and Data Link Section.
- The GPS System - Sources of Errors in GPS*. (2009, 04 19). Tratto da www.kowoma.de: <http://www.kowoma.de/en/gps/errors.htm>
- Welch, G., & Bishop, G. (2006). *An Introduction to the Kalman Filter*. Chapel Hill.
- Wieser, A., & Gebre-Egziabher, D. (2007, January/February). Weighting GNSS observations and variations of GNSS/INS integration. *GNSS Solutions* .
- Wikipedia - Accelerometer*. (2010). Tratto da www.wikipedia.com: www.wikipedia.com
- Wikipedia - Variance*. (2010). Tratto da www.wikipedia.org.
- Woodman, O. J. (2007). *An introduction to inertial navigation*. Technical Report, University of Cambridge, Computer laboratory.
- Xsens. (2007). *MTi and MTx User Manual and Technical Documentation*.